International Journal of Solids and Structures 46 (2009) 4006–4024

Contents lists available at ScienceDirect

International Journal of Solids and Structures

journal homepage: www.elsevier.com/locate/ijsolstr

A new theoretical approach for structural modelling of riveted and spot welded multi-spot structures

Francesco Vivio *

Department of Mechanical Engineering, University of Rome "Tor Vergata", Via del Politecnico 1, 00133 Rome, Italy

ARTICLE INFO

Article history:
Received 28 February 2009
Received in revised form 14 July 2009
Available online 4 August 2009

Keywords:
Spot weld
Rivet
Analytical method
Closed form solutions
Local stiffness evaluation, Stress analysis

ABSTRACT

A general theoretical approach based on theory of elasticity is presented in order to define the structural behaviour of riveted and spot welded joints. The new closed form solutions lead to the definition of a joint element useful to FE models of riveted or spot welded multi-spot structures. The objective is an accurate evaluation of the local elastic stiffness of spot joints in FE analysis, which is fundamental to perform a reliable simulation of multi-joint structures and, consequently, a good estimate of loads acting on spots; this makes it possible to introduce structural stress or new general criteria allowing, for example, to predict fatigue behaviour. On the other hand, a low entry of degrees of freedom is needed when several spot joints are present in a complex structure. The goal is to reach a reliable spot region model which can be used as the basis to develop a spot element in FE analysis. In the present paper, based on new closed form solutions, a spot element is introduced, so as to precisely evaluate both local and overall stiffness both of spot welded joints and riveted joints. Based on the stress function approach and the Kirchhoff plate theory in linear elastic hypotheses, closed-form in-plane stress, displacement, moment and transverse shear force solutions are derived for a new bidimensional model, subjected to various types of loads. The capability to simulate spot welds or rivets depends on the definition of two elastic parameters intrinsic in closed form solutions, that tunes the theoretical model according to actual joint behaviour.

The proposed joint element combines the precision in the simulation with a very limited number degrees of freedom in the overall finite element model of an actual multi-spot structure.

The results obtained using the introduced theoretical framework and spot element approach perfectly match those obtained using very refined FE models and experimental data.

1. Introduction

The interest on structures jointed by spot welds and rivets has been recently spreading especially in automotive, railways applications and aeronautical structures, where structures may contain several thousands of spot joints.

These spot joints are generally subjected to complex multiaxial loads. Structural behaviour and local stiffness evaluation of spot joints show some complexity, due to the difficulties in accurate modelling the region close to each spot joint, featuring local high stress/strain, associated with very high stress/strain gradients. The stress field close to the spot region is quite complex, mostly due to geometrical irregularities and several local effects at the edge of the spot joint.

Furthermore, it is necessary to use models that involve only a few degrees of freedom, since real structures usually contain several spot welds: modelling each of them with accurate and complex FE models would require a major computational effort. However, when modelling actual structures with several spot joints, it is essential to make use of drastic simplifications, which have a considerable impact on results. In fact, several approaches were proposed in the past, which introduced various degrees of simplification replacing the spot weld with a single beam element or a rigid bar.

The studies about spot weld junction behaviour are mainly focused on problems of fatigue life evaluation. Fatigue life estimation has been investigated using different approaches. Generally, a major effort has been made so as to obtain stresses at the spot welds, using finite element models, theoretical approach, experimental evidence or any combination of the above. Often, fracture mechanics has been used to evaluate stress intensity factors in natural crack or notch along the nugget circumference. In this case, various types of simple specimens have been investigated using finite element models in linear elastic conditions (Sheppard, 1993; Wang et al., 2005), in elastic–plastic conditions (Satoh et al., 1991; Deng et al., 2000; Pan and Sheppard, 2002), approximate analytical solutions for stress intensity factor (Zhang, 1997, 2001; Lin et al., 2007) or complete analytical solutions (Lin and Pan, 2008a,b), again for stress intensity factor. Structural stress approach has been

* Tel.: +39 06 72597123; fax: +39 06 2021351.
E-mail address: vivio@uniroma2.it.

0020-7683/$ - see front matter © 2009 Elsevier Ltd. All rights reserved.
doi:10.1016/j.ijsolstr.2009.07.021

introduced to predict fatigue life (Radaj, 1990; Radaj and Soegiharto, 1990) using stress intensity factor. It should also be noted that in these cases fatigue behaviour models are often only applicable and valid for reference joints of simple shape. Otherwise the use of a conventional stress parameter has been proposed (Rupp et al., 1990, 1995; Salvini et al., 1997, 2000) demonstrating its effectiveness to predict spot weld fatigue life. In this case, simple models can lead to a good estimate of the loads interchanged between the spot weld and the rest of the structure, and these loads can be related to a conventional stress parameter at the spot weld by simple theoretical models (Rupp et al., 1990, 1995) or theoretical models (Salvini et al., 1997, 2000). Nevertheless, whatever the used approach the priority is the correct evaluation of local joint stiffness that drives to a fined evaluation of stress field in this region.

Riveting is a well established technology in the manufacturing of aeronautical structures as well as in the automotive industries. This technology is a simple and versatile solution when low thickness sheets are connected, especially when lightweight alloys are used.

Even for riveted joints, refined models of the region around rivets, requiring 3D models and the use of contact elements (Urban, 2003; Al-Emrani and Kliger, 2003), which causes considerable time consuming in multi-joint structure analyses, are employed. Even when dealing with non linear analyses carried out with explicit FE codes, for crashworthiness analysis purposes, 3D complex models are proposed (Langrand et al., 2001). This requirement considerably discourages the extension of the analysis to multi-riveted structures. On the other side, the use of simplified models – use of mono-dimensional links, action of kinematic constraints (Karaoğlu and Kuralay, 2002), non linear elastic links, mixed methods (Langrand et al., 2001) – only achieves a poor approximation of the actual behaviour in terms of local stiffness. Some 2D models that make use of spring and gap elements have also been proposed (Xiong and Bedair, 1999), which are often referenced with analytical solutions allowing to evaluate the local stress field in the surrounding region of each joint.

On the basis of the above, when modelling actual structures with several spot joints, it is essential to make use of drastic simplifications, which have a considerable impact on results. The main need for such an accurate definition of the stiffness of the spot area leads to accurately evaluating loads on spot joints.

To overcome such limitations, a method based on a theoretical solution of the region close to the spot weld has been proposed by Salvini et al. (2000) and Vivio et al. (2002). The spot weld element approach proposed in these papers constitutes an efficient way of modelling the spot weld in FE solutions, using a complete stiffness characterization of spot weld region – condensed on the nodes that surround the spot – using a closed-form solution of a reference theoretical model (a circular plate with a central rigid inclusion).

The model features a set of equivalent radial beam, with six degrees of freedom per node, lying on metal sheet, and a central beam element (main link) representing the spot weld nugget and connecting the two metal sheets. The spot element introduces a very small number of degrees of freedom and the improvements in accuracy of results – under the elastic hypothesis – are apparent when a comparison with other modelling techniques is performed, as demonstrated by Vivio et al. (2002) and confirmed by Palmonella et al. (2005). Vivio and Fanelli (2009) also introduced an analytical procedure for the evaluation of the elastic–plastic behaviour of spot welded joints, subjected to orthogonal load, that can be used to develop the spot weld element approach in FE analysis when plasticity and large deflections are in effect.

In this paper, a new theoretical framework is proposed in order to describe the elastic behaviour of spot joints (spot welds or rivets) under various types of loading conditions.

A more general and refined reference model, based on the one used for spot weld element definition in linear elastic hypothesis, is here introduced. Here the rigid nugget and the circular plate are connected with appropriate boundary connections providing a tuned rotational stiffness (in radial direction). The new version of the theoretical reference model proposed here is composed by a circular thin plate containing a rigid central region (shank of rivet or spot weld core), elastically connected in correspondence of the interface, and clamped at the external radius. A scheme of it is shown in Fig. 1.

Varying boundary connections between central rigid nugget and the inner radius of the plate by using a tuned rotational stiffness in radial direction, it is possible to define the spot weld model (considering a rigid connection between rigid nugget and plate) and rivet model (considering a variable flexible connection between rigid nugget and plate).

The analytical solution of the theoretical reference model is found through two kind of solutions: (i) by integration of the elliptic equations that resolve bending plate problems, when the plate is subjected to bending moments and/or out-of-plane loads; (ii) by integration of the elliptic equations that characterize the in-plane membrane problem subjected to tangential loads. The theoretical model is studied taking into account of the main load that can act on a joint as applied to the central rigid core (Fig. 1). The purpose is to fully characterize the structural behaviour, so that a new equivalent element assembly (the Spot Element) can be defined.

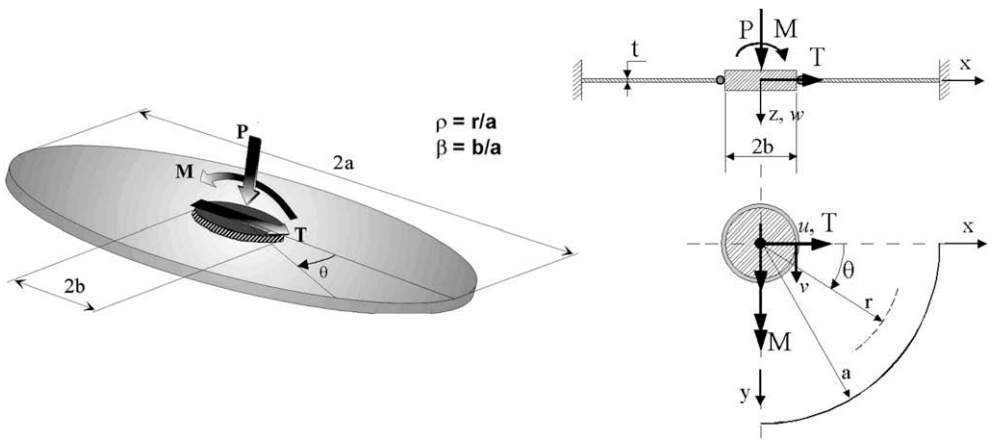

Fig. 1. Theoretical model of spot joint with elastic connection between central nugget and plate.

The spot element assembly, based on the analytical solution, can be then defined using the strategy approached by Vivio et al. (2002). The spot element is carried out by means of an assembly of beam elements provided of rigid offsets, radially disposed and properly connected each other. Each node of main link is connected to the chosen shell nodes of the two plates by radial beams showing a rigid part and a flexible part.

Elastic characteristics of beam elements are computed through the solution of a set of equations, afterwards described, representing the structural equivalence (in terms of stiffness between rigid core and circular boundary nodes) of the beams assembly versus the reference theoretical model.

Actually there are multiple riveting techniques (many types of pop rivets, self-piercing rivets, etc.) in the different fields of application. A relevant advantage of the present approach is that only two parameters (κ and ζ, introduced later) are able to differentiate the joining local stiffness according to the spot weld present or to the effective riveting techniques. In this version of the element, both effects due to contact in riveted joints (existence of gap and friction between the rivets and the metal sheets) and local stress concentration effects, as experienced by Ho and Chau (1997), are not accounted. However, the correct evaluation of the local and global stiffness of multi-spot structures is to be considered as a crucial preliminary step, before evaluating the effective stress and strain field.

The use of the proposed joint element, allowing for great precision in the simulation with limited number degrees of freedom in the overall finite element model, allows to correctly evaluate all load acting on spots. The correct evaluation of loads allows to evaluate local stress or structural stress around rivets or spot welds, using closed form solutions presented here as well as other solutions available in literature.

The results obtained using the introduced theoretical framework and spot element approach have been validated by comparing with those obtained by reference specimen models performed using very complex and refined FE models, and experimental data.

2. Definition of the assembled spot element

The assembled spot element is formed by two sub-elements, each consisting of the theoretical model of Fig. 1.

To adapt the bi-dimensional analytical solution to a discretized one-dimensional model, it is necessary to apply adequate stiffness values between the central node (node 1) and all the peripheral nodes of the spot element (named nodes 2); stiffness values are therefore associated to a determined bi-dimensional circular sector (Fig. 2). The structural behaviour of the assembly leads to the desired equivalence with the analytical model.

The closed-form solution of the circular plate with central rigid inclusion in all loading conditions can be condensed onto the nodes contouring the spot region using the general definition of stiffness: the ratio of applied force to measured displacement when all remaining dofs are restrained.

Given that analytical solutions – explained later – either do not depend on θ in *P*-load or depend sinusoidally on θ, it is sufficient to consider only the circular sector (Fig. 2) where the quantities assume their maximum value on θ (Vivio et al., 2002).

In order to introduce a procedure using simple one-dimensional elements which already exist in all commercial codes, the condensed element representing spot surrounding region is translated into a series of two coupled radial beams, appropriately linked together, as shown in Fig. 2. This single couple of beams globally shows the same stiffness of the circular sector of the theoretical model, having $\alpha_1 + \alpha_2$ angular extension (Fig. 2), with considerable accuracy. Type 1 beams T_1 are connected through rigid offsets at both ends, whereas type 2 beams T_2 do not show any offsets. The use of an appropriate linking between T_1 beam and T_2 beam is necessary in order to avoid the expected coupling between *P*-load and *M*-load stiffness terms, as synthesized in Fig. 2; the chosen assembly and constraints cause the T_2 beams react only to orthogonal load on node 2 when a generic displacement is applied on node 1.

Nevertheless, although the whole spot element assembly is not trivial, the procedure is repetitive and a macro may be easily created for use as an add-on in any commercial finite element code.

For any couple of beams 1 and 2, referenced to the circular sector having $\alpha_1 + \alpha_2$ angular extension, six equivalence conditions between stiffness terms – having *th* apex – given by the theoretical model (in terms of ratio of resulting generic force at the peripheral node 2 to generic displacement at node 1) and stiffness terms – having *beam* apex – of the beam groups may be written as follows:

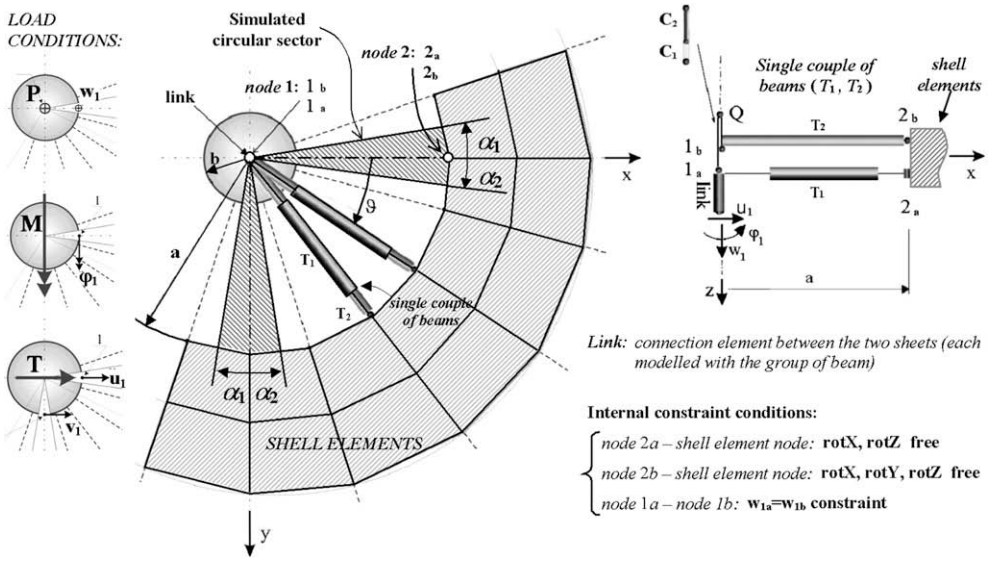

Fig. 2. Scheme of Spot Element: general conditions and assembling definition for each pair of beams.

$$\begin{cases} K^{th}_{Pw}(\kappa) = K^{beam1}_{Pw}(J_{z1}, x_i, x_j) + K^{beam2}_{Pw}(J_{z2}) \\ K^{th}_{Mw}(\kappa) = K^{beam1}_{Mw}(J_{z1}, x_i, x_j) \\ K^{th}_{P\varphi}(\kappa) = K^{beam1}_{P\varphi}(J_{z1}, x_i, x_j) \\ K^{th}_{M\varphi}(\kappa) = K^{beam1}_{M\varphi}(J_{z1}, x_i, x_j) \\ K^{th}_{Fn_u}(\zeta) = K^{beam1}_{Fn_u}(J_{y1}) \\ K^{th}_{Ft_v}(\zeta) = K^{beam1}_{Ft_v}(A_1) \end{cases} \quad (1)$$

The generic forces at the peripheral node 2 are radial bending moment (apex M), orthogonal load (apex P), in plane radial (apex F_n) and tangential forces (apex F_t), while the generic displacements at the central node 1 are deflection along z-axis (apex w), rotation (apex φ), in plane radial (apex u) and tangential displacements (apex v). Theoretical terms, derived from the analytical solution, are also function of κ and ζ, parameter in order to consider spot weld simulation or rivet simulation, as hereinafter described. The terms of beam with rigid offset (T_1 beam) depend on five unknown parameters: inertia moments $J_{y1}$and J_{z1}, area A_1 and rigid offset lengths x_i and x_j; the unique term of beam without offset (T_2 beam) depends on its inertia moment J_{z2} (the sixth unknown parameter).

The structural equivalence synthesized by Eq. (1) is valid for any combination of bending moments, in-plane loads and off plane loads applied to the spot nugget, and provides the values of the six unknown equivalent parameter.

Note that only a further stiffness contribution is given by T_2 beam (only in first condition of Eq. (1)) since this beam reacts only with orthogonal load on node 2 when a generic displacement is applied on node 1.

The contribution of T_2 beam in the local stiffness can be analysed, using the first condition of Eq. (1) and analytical relations of stiffness terms of theoretical model (mentioned in following Sections 3.1 and 3.2) and considering that $a \cdot K^{beam1}_{Pw} = K^{beam1}_{Mw} + K^{beam1}_{P\varphi} = K^{th}_{Mw} + K^{th}_{P\varphi}$. It is possible to demonstrate that the influence of T_2 beam stiffness K^{beam2}_{Pw}, if compared to T_1 beam stiffness K^{beam1}_{Pw}, becomes negligible – for every value of κ – when β assumes the most used values ($0.2 < \beta < 1$) in modelling spot jointed structures. In this case T_2 beam can be omitted on spot element assembly.

The actual connection between the two metal sheets is guaranteed by the *link* (Fig. 2) element, which is set with the material and the geometrical characteristics of the spot weld core or of the rivet shank. An appropriate definition of equivalent mechanical properties of this element make it possible to consider decreasing the spot properties due to progressive damage or breaking, as discussed in Salvini et al. (2000) and Vivio et al. (2002) for spot weld elements. The final rupture of the rivet or of the spot weld may correspond to a total link elimination.

The assembled spot element can be inserted into the global joint FE model so as to replace the hole left by the removed region surrounding the spot or rivet.

The analytical solution, extended to circumferential portions of the circular region surrounding the nuggets, also allows to deal with non-regular-shaped mesh (Vivio et al., 2002). Note that the shape of the region surrounding the spot was assumed as circular; however, the generic definition of the model (in order to compute the stiffness of each sector) also allows for managing non-circular spot regions. In this case it is possible to discretize the spot region considering the subdivision of sectors for a generic non-circular bordered spot element (Fig. 3).

The stiffness estimate of a i-th span sector, having an angular extension $\alpha_i/2 + \alpha_{i+1}/2$, is performed using the theoretical model of Fig. 1 having outer radius a_i, equal to the distance between master node and the i-th peripheral node. The stiffnesses of each sector which do not depend on θ; as hereinafter described, and the analytical solution of the i-th circumferential portions of the circular region surrounding the nuggets make it possible to define the corresponding couple of beams T_1 and T_2 (Fig. 2).

Global stiffness behaviour of non-circular spot element s is therefore as simple to compute as circular shapes; obviously, accuracy increases with number of nodes on the spot contour (and, consequently, sector span angles decrease), according to global mesh requirements.

Note that the link can be located anywhere between the parts that are to be connected, in the actual centre of the spot weld, independent of the mesh and the node locations.

The spot element assembly formulation, even if it makes use of elaborate procedures, is although rather repetitive to apply; therefore a macro may be easily created as add-on on any commercial finite element code.

3. Theoretical solution

The stiffness terms of the spot joint are analytically computed by means of the closed-form solutions of the bi-dimensional model mentioned above (Fig. 1). The outer radius of the plate ($r = a$) is clamped and the central inclusion is constrained at the inner radius ($r = b$) of the plate, with a variable radial stiffness. The same figure shows the polar coordinate system (r, θ, z). The rigid core is loaded with bending moment M, orthogonal load P and in-plane load T.

In the following sections, closed-form solutions are all presented, focussing the attention on the displacement field, constraint loads, and displacement at the central nugget. All these quantities are essential to define the theoretical stiffness of the spot element, either for spot weld or for rivet version.

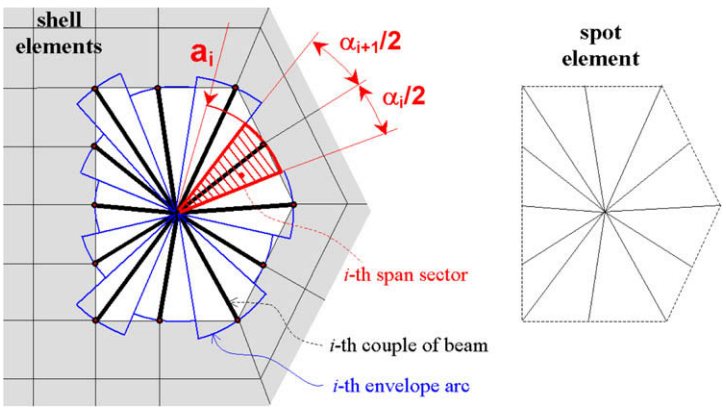

Fig. 3. Managing of a generic shape of Spot Element into a shell FE model.

3.1. Bending moment M

This load condition represents a spot joint under central bending conditions. The bending moment M is applied to the nugget centre and it is represented by a vector laying in the sheet plane (Fig. 1). According to Kirchhoff plate theory (Timoshenko and Woinowsky-Krieger, 1959) the differential equation governing the elastic solution for a bending plate non subjected to distributed loads in polar coordinates (r,θ) is:

$$\Delta\Delta w = \left(\frac{\partial^2}{\partial r^2}+\frac{1}{r}\frac{\partial}{\partial r}+\frac{1}{r^2}\frac{\partial}{\partial \theta^2}\right)\left(\frac{\partial^2 w}{\partial r^2}+\frac{1}{r}\frac{\partial w}{\partial r}+\frac{1}{r^2}\frac{\partial^2 w}{\partial \theta^2}\right)=0, \tag{2}$$

where $w(r,\theta)$ is the deflection along z-axis direction, and Δ is the harmonic operator.

Defining the dimensionless radius as $\rho = r/a$ and considering the ratio $\beta = b/a$, the four boundary conditions to impose to the model are:

$$\begin{aligned}&(a): (w)_{\rho=1}=0;\ (b): \left(\frac{\partial w}{\partial \rho}\right)_{\rho=1}=0;\ (c): M_r|_{\rho=\beta}=\kappa\\ &\quad M^*_M(\theta),\ \text{with } 0\leqslant\kappa\leqslant 1\\ &(d): a\int_{-\pi}^{\pi}(M_r)_{\rho=1}\cos\theta d\theta - a\int_{-\pi}^{\pi}(M_{rt})_{\rho=1}\sin\theta d\theta + a^2\int_{-\pi}^{\pi}(Q_r)_{\rho=1}\\ &\quad \cos\theta d\theta + M = 0.\end{aligned} \tag{3}$$

where κ is the parameter that differentiates the joining local stiffness, $\varphi = -1/a\partial w/\partial\rho$ is the rotation angle of the normal to the deflection middle surface of the plate in the diametral section, M_r is the radial moment, M_{rt} is the twisting moment, Q_r is the radial shearing force while $M^*_M(\theta)$is the clamping radial moment between the rigid nugget and the plate when a clamping is accounted

$$M^*_M(\theta) = \frac{M}{2\pi a}\frac{(\beta^2-1)}{\beta(\beta^2+1)}\cos\theta. \tag{4}$$

This reaction moment $M^*_M(\theta)$can be computed by solving the differential Eq. (2) with the boundary conditions (a), (b) and (d) of Eq. (3) and the clamping condition at the inner radius

$$[\partial w/\partial\rho]_{\rho=\beta} = [w/\rho]_{\rho=\beta} \tag{5}$$

instead of condition (c) of Eq. (3).

The general characterisation of the spot model, which allows to manage the actual constraint conditions between the nugget and the metal sheets, is useful to define a spot weld model or a general rivet model. To this end, the boundary condition (c) of Eq. (3) represent an elastic radial stiffness between rigid nugget and plate, where a rigid rotation occurs. This position is intermediate between pure clamping (characterized by the condition (5)) – which corresponds to the spot weld condition – and pure hinging (characterized by the $M_r|_{\rho=\beta}=0$). Spot weld condition can be achieved by putting $\kappa = 1$ while the generic rivet condition can be achieved by putting $0\leqslant\kappa<1$.

Using boundary conditions (3) it is possible to compute the displacement field all over the plate, which is needed to define analytical stiffness in the region surrounding the generic spot joint as a function of the κ parameter, which is a term that tunes the elastic connection between the nugget and the inner radius of the sheet.

The general solution of w in Eq. (4) is:

$$w(r,\theta) = w_0(r,\theta) = R_0 + \sum_{m=1}^{\infty} R_m\cdot\cos m\theta + \sum_{m=1}^{\infty} R'_m\cdot\sin m\theta \tag{6}$$

where $R_0, R_1, R_2, \ldots, R_m, R'_1, R'_2, \ldots, R'_m$ are functions of r, independent of θ. The number of terms appearing in the series depends on the periodical shape of the boundary conditions. Here, R_0, R_1, R_m and R'_m terms are

$$\begin{cases} R_0(r) = A_0 + B_0 r^2 + C_0\log r + D_0 r^2\log r;\\ R_1(r) = A_1 r + B_1 r^3 + C_1 r^{-1} + D_1 r\log r;\\ \ldots\\ R_m(r) = A_m r^m + B_m r^{-m} + C_m r^{m+2} + D_m r^{-m+2};\quad m>1\\ R'_1(r) = A'_1 r + B'_1 r^3 + C'_1 r^{-1} + D'_1 r\log r;\\ \ldots\\ R'_m(r) = A'_m r^m + B'_m r^{-m} + C'_m r^{m+2} + D'_m r^{-m+2};\quad m>1. \end{cases} \tag{7}$$

Substituting Eq. (7) into Eq. (6) the general solution of deflection $w(r,\theta)$ is obtained. In the case here examined, involving a circular plate with central rigid nugget, subjected to an external bending moment M, the solution expressed by Eq. (6) simplifies. In fact, the R_0 term vanishes since the external load does not include an axial symmetric component; furthermore, the θ values are measured from the reference plane where the external moment acts (Fig. 1). Therefore, the M_r solution series is limited to the simple cosinusoidal component. The deflection w has only a cosinusoidal term and the only term of R_i and R'_i different from zero is R_1. Therefore, the solution of deflection w is the following:

$$\begin{aligned} w(\rho,\theta) &= R_1(\rho)\cos\theta\\ &= \left(A_1\rho + B_1\rho^3 + C_1\rho^{-1} + D_1\rho\log\rho\right)\cdot\cos\theta. \end{aligned} \tag{8}$$

The unknown coefficients A_1, B_1, C_1 and D_1 can be determined by imposing the boundary conditions (3).

In the polar coordinate system, the general relationships between the deflection $w(r,\theta)$ and moments and transverse shear forces, in terms of r and θ, are:

$$\begin{aligned} M_r(r,\theta) = &-D\left[\frac{\partial^2 w}{\partial r^2}(\cos^2\theta + \nu\sin^2\theta) + \left(\frac{1}{r}\frac{\partial w}{\partial r}+\frac{1}{r^2}\frac{\partial^2 w}{\partial\vartheta^2}\right)\right.\\ &\times(\sin^2\theta+\nu\cos^2\theta) + 2(1-\nu)\left(\frac{1}{r^2}\frac{\partial w}{\partial\theta}-\frac{1}{r}\frac{\partial^2 w}{\partial r\cdot\partial\theta}\right)\\ &\left.\times\sin\theta\cos\theta\right]; \end{aligned} \tag{6a}$$

$$\begin{aligned} M_t(r,\theta) = -D\left[\frac{\partial^2 w}{\partial r^2}(\sin^2\theta+\nu\cos^2\theta)+\left(\frac{1}{r}\frac{\partial w}{\partial r}+\frac{1}{r^2}\frac{\partial^2 w}{\partial\theta^2}\right)\right.\\ \left.\times(\cos^2\theta+\nu\sin^2\theta)+-2(1-\nu)\left(\frac{1}{r^2}\frac{\partial w}{\partial\theta}-\frac{1}{r}\frac{\partial^2 w}{\partial r\partial\theta}\right)\sin\theta\cos\theta\right]; \end{aligned} \tag{6b}$$

$$\begin{aligned} M_{rt}(r,\theta) = D(1-\nu)\left[\left(\frac{\partial^2 w}{\partial r^2}-\frac{1}{r}\frac{\partial w}{\partial r}-\frac{1}{r^2}\frac{\partial^2 w}{\partial\theta^2}\right)\frac{\sin 2\theta}{2}\right.\\ \left.+\left(\frac{1}{r}\frac{\partial^2 w}{\partial r\partial\theta}-\frac{1}{r^2}\frac{\partial w}{\partial\theta}\right)\cos 2\theta\right]; \end{aligned} \tag{6c}$$

$$Q_r(r,\theta) = -D\frac{\partial}{\partial r}(\Delta w) = -D\frac{\partial}{\partial r}\left(\frac{\partial^2 w}{\partial r^2}+\frac{1}{r}\frac{\partial w}{\partial r}+\frac{1}{r^2}\frac{\partial^2 w}{\partial\theta^2}\right); \tag{6d}$$

$$Q_t(r,\theta) = -D\frac{1}{r}\frac{\partial(\Delta w)}{\partial\theta} = -D\frac{1}{r}\frac{\partial}{\partial\theta}\left(\frac{\partial^2 w}{\partial r^2}+\frac{1}{r}\frac{\partial w}{\partial r}+\frac{1}{r^2}\frac{\partial^2 w}{\partial\theta^2}\right), \tag{6e}$$

where M_t is the tangential bending moment, Q_t is the tangential shearing force and $D = Et^3/12(1-\nu^2)$ is the flexural rigidity of the plate, whose thickness is t, E is Young's modulus and ν is Poisson's ratio.

It is straightforward to derive the closed-form solutions of this model in terms of κ parameter; the deflection $w(\rho,\theta)$ and the rotation of a segment initially orthogonal to the plate in a point $\varphi(\rho,\theta)$, are:

$$w(\rho,\theta)=\frac{aM\cos\theta\{(3+\nu)[\rho^2(1-2\ln\rho)-1]\beta^4+(1+\nu)(\rho^2-1)^2\beta^2+(1+2\ln\rho)(\nu-1)\rho^2+(1-\nu)\rho^4\}}{8\pi D\rho[(\nu-1)-(3+\nu)\beta^4]}+\kappa\frac{aM\cos\theta\beta^2(\beta^2-1)(\rho^2-1)^2}{4\pi D\rho(\beta^2+1)[(\nu-1)-(3+\nu)\beta^4]}. \tag{7a}$$

$$\varphi(\rho,\theta)=-\frac{1}{a}\frac{\partial w}{\partial\rho}=\frac{M\cos\theta\{(3+\nu)[-1+\rho^2(1+2\ln\rho)]\beta^4+(1+\nu)(-3\rho^4+2\rho^2+1)\beta^2+(1-\nu)[-3\rho^4+(2\ln\rho+3)\rho^2]\}}{8\pi D\rho^2[(-1+\nu)-(3+\nu)\beta^4]}-\kappa\frac{aM\cos\theta\beta^2(\beta^2-1)(3\rho^2+1)(\rho^2-1)}{4\pi D\rho^2(\beta^2+1)[(\nu-1)-(3+\nu)\beta^4]}. \tag{7b}$$

The moments and shear forces of this model are given as:

$$M_r(\rho,\theta)=\frac{M\cos\theta(\rho^2-\beta^2)(\nu-1)[(3+\nu)\rho^2\beta^2-(3+\nu)(\beta^2+\rho^2)+\nu+1]}{4\pi a\rho^3[(3+\nu)\beta^4+(1-\nu)]}+\kappa\frac{M\cos\theta\beta^2(\beta^2-1)[(3+\nu)\rho^4+(1-\nu)]}{2\pi a\rho^3(\beta^2+1)[(3+\nu)\beta^4+(1-\nu)]}. \tag{8a}$$

$$M_t(\rho,\theta)=\frac{M\cos\theta\{(3+\nu)\beta^4[(1+\nu)\rho^2-(1-\nu)]-(1+3\nu)\rho^4[(\nu+1)\beta^2+(1-\nu)]-(\nu^2-1)(\beta^2+\rho^2)\}}{4\pi a\rho^3[(3+\nu)\beta^4+(1-\nu)]}+\kappa\frac{M\cos\theta\beta^2(\beta^2-1)[(1+3\nu)\rho^4-(1-\nu)]}{2\pi a\rho^3(\beta^2+1)[(3+\nu)\beta^4+(1-\nu)]}. \tag{8b}$$

$$M_{rt}(\rho,\theta)=\frac{M\sin\theta(1-\nu)(\rho^2-1)[(1-\nu)\rho^2+(1+\nu)\beta^2(\rho^2+1)+(3+\nu)\beta^4]}{4\pi a\rho^3[(3+\nu)\beta^4+(1-\nu)]}+\kappa\frac{M\sin\theta(1-\nu)\beta^2(\beta^2-1)(\rho^4-1)}{2\pi a\rho^3(\beta^2+1)[(3+\nu)\beta^4+(1-\nu)]}. \tag{8c}$$

$$Q_r(\rho,\theta)=\frac{M\cos\theta[2(1-\nu)\rho^2+2(1+\nu)\beta^2+(3+\nu)\beta^4+(1-\nu)]}{2\pi a^2\rho^2[(3+\nu)\beta^4+(1-\nu)]}-\kappa\frac{2M\cos\theta\beta^2(\beta^2-1)}{\pi a^2(\beta^2+1)[(3+\nu)\beta^4+(1-\nu)]}; \tag{8d}$$

$$Q_t(\rho,\theta)=\frac{M\sin\theta[2(\nu-1)\rho^2-2(1+\nu)\beta^2+(3+\nu)\beta^4+(1-\nu)]}{2\pi a^2\rho^2[(3+\nu)\beta^4+(1-\nu)]}-\kappa\frac{2M\sin\theta\beta^2(\beta^2-1)}{\pi a^2(\beta^2+1)[(3+\nu)\beta^4+(1-\nu)]}. \tag{8e}$$

In Fig. 4 the theoretical results, in dimensionless form, are shown in a reference geometry given within the picture itself ($E=200$ GPa, $\nu=0.3$), using dimensionless $\bar{\rho}=(\rho-\beta)/(1-\beta)$ variable. The κ connecting condition constant and β ratio are used, separately, as parameter. Varying the κ connecting condition, a family of characteristics – smoothly changing – is found. Moreover, by referring to functions in Fig. 4, we have that $M_r(\beta,0)$ and $\varphi(\beta,0)$ tend to infinity for $\beta\to 0$.

Note that the stresses for the spot under a resultant bending moment acting along x axis can be obtained by substituting $\theta+\pi/2$ for θ in Eqs. (7) and (8).

In order to introduce the spot element representing the spot joint and its surrounding region it is possible to define the stiffness $K^{th}_{M\varphi}(\kappa)$ and $K^{th}_{P\varphi}(\kappa)$ of Eq. (1) by the ratio of resulting generic force at the peripheral node and the slope of the rigid nugget:

$$K^{th}_{P\varphi}(\kappa)=\frac{\int_{-\alpha_1}^{\alpha_2}aQ_r(1,0)\cos\theta d\theta}{\varphi(\beta,0)}=\frac{F_2}{\varphi_1}=\frac{1}{a}\frac{2D[\kappa_4\beta^2(\beta^2-1)+(3+\nu)\beta^6+(3\nu+5)\beta^4+(5-\nu)\beta^2+3(1-\nu)](\sin\alpha_1+\sin\alpha_2)}{\kappa(\beta-1)^3(\beta+1)^3-\ln\beta(\beta^2+1)[\beta^4(3+\nu)+(1-\nu)]+[\beta^2(2+\nu)-\nu](\beta^4-1)}. \tag{9}$$

$$K^{th}_{M\varphi}(\kappa)=\frac{\int_{-\alpha_1}^{\alpha_2}aM_r(1,0)\cos\theta d\theta}{\varphi_1(\beta,0)}=\frac{M_2}{\varphi_1}=\frac{2D(\beta^2-1)[(1-\kappa)4\beta^2+(3+\nu)\beta^4+(1-\nu)](\sin\alpha_1+\sin\alpha_2)}{\kappa(\beta-1)^3(\beta+1)^3-\ln\beta(\beta^2+1)[\beta^4(3+\nu)+(1-\nu)]+[\beta^2(2+\nu)-\nu](\beta^4-1)}. \tag{10}$$

where $\varphi(\beta,0)$, is the maximum values on θ of the rotations in correspondence of the rigid nugget, $M_r(1,0)$ e $Q_r(1,0)$ are the maximum values on θ of the reaction loads at the outer radius; $K^{th}_{P\varphi}(\kappa)$ is the ratio between the resultant radial shearing force on the outer border of the circular sector having extension $\alpha_1+\alpha_2$ (see Fig. 2) and the rotation at the nugget edge; $K^{th}_{M\varphi}(\kappa)$ is the ratio between the resultant radial moment on the above-mentioned outer border of the circular sector and the rotation at the nugget edge.

Note that the stiffness functions $K^{th}_{P\varphi}(\kappa)$ and $K^{th}_{M\varphi}(\kappa)$ do not depend on θ and they are valid for every direction of application of the resultant bending moment.

Fig. 5 shows the curves of dimensionless stiffnesses $\overline{K}_{P\varphi}=K^{th}_{P\varphi}\cdot a/D(\sin\alpha_1+\sin\alpha_2)$ and $\overline{K}_{M\varphi}=K^{th}_{M\varphi}/D(\sin\alpha_1+\sin\alpha_2)$ as function of β, for various values of κ parameter and $\nu=0.3$. By referring to functions in Fig. 5, it is confirmed that $\overline{K}_{P\varphi}$ and $\overline{K}_{M\varphi}$ increase with β ratio and tend to infinity when the inner radius of the reference model tends to its outer radius ($\beta\to 1$).

3.2. Orthogonal load P

This model represents a spot joint under opening loading conditions. The orthogonal load P acts along the axis of the rigid nugget (Fig. 1). In this case, the problem is axisymmetric so that solutions are one-dimensional (r). The differential Eq. (2), when all derivatives of θ disappear, assumes the form:

$$\frac{d}{dr}\left[\frac{1}{r}\frac{d}{dr}\left(r\frac{dw}{dr}\right)\right]=\frac{Q_r}{D}. \tag{11}$$

where $Q_r=P/2\pi r$ is the shearing force on r.

Using the dimensionless variable ρ , the boundary conditions are now:

$$\begin{aligned}&(a): w|_{\rho=1}=0;\\ &(b): \frac{dw}{d\rho}|_{\rho=1}=0;\\ &(c): M_r|_{\rho=\beta}=\kappa M^*_P;\quad 0<\kappa<1,\end{aligned} \tag{12}$$

where M^*_P is the clamping radial moment between the rigid nugget and the plate when a clamping is accounted

$$M^*_P=\frac{P}{4\pi}\left[\frac{2\ln(\beta)}{(\beta^2-1)}-1\right]. \tag{13}$$

This reaction moment M^*_P can be computed by solving the differential Eq. (11) with the boundary conditions (a), (b) of Eq. (12) and the clamping condition at the inner radius

$$[\partial w/\partial\rho]_{\rho=\beta}=[w/\rho]_{\rho=\beta} \tag{14}$$

instead of condition (c) of Eq. (12).

Even here, using boundary conditions (12) it is possible to compute the displacement field all over the plate, necessary to define the analytical stiffness in the region surrounding the generic spot joint as a function of the κ parameter.

It is straightforward to derive the closed-form solutions of this model in terms of the κ parameter; the deflection $w(\rho)$ and the rotation $\varphi(\rho)$ are:

$$w(\rho)=\frac{a^2P}{16\pi D}\frac{N_{WP}+2\kappa^2_\beta[(\rho^2-2ln\rho-1)(\beta^2-2ln\beta-1)]}{[(1+\nu)\beta^2+1-\nu]};$$

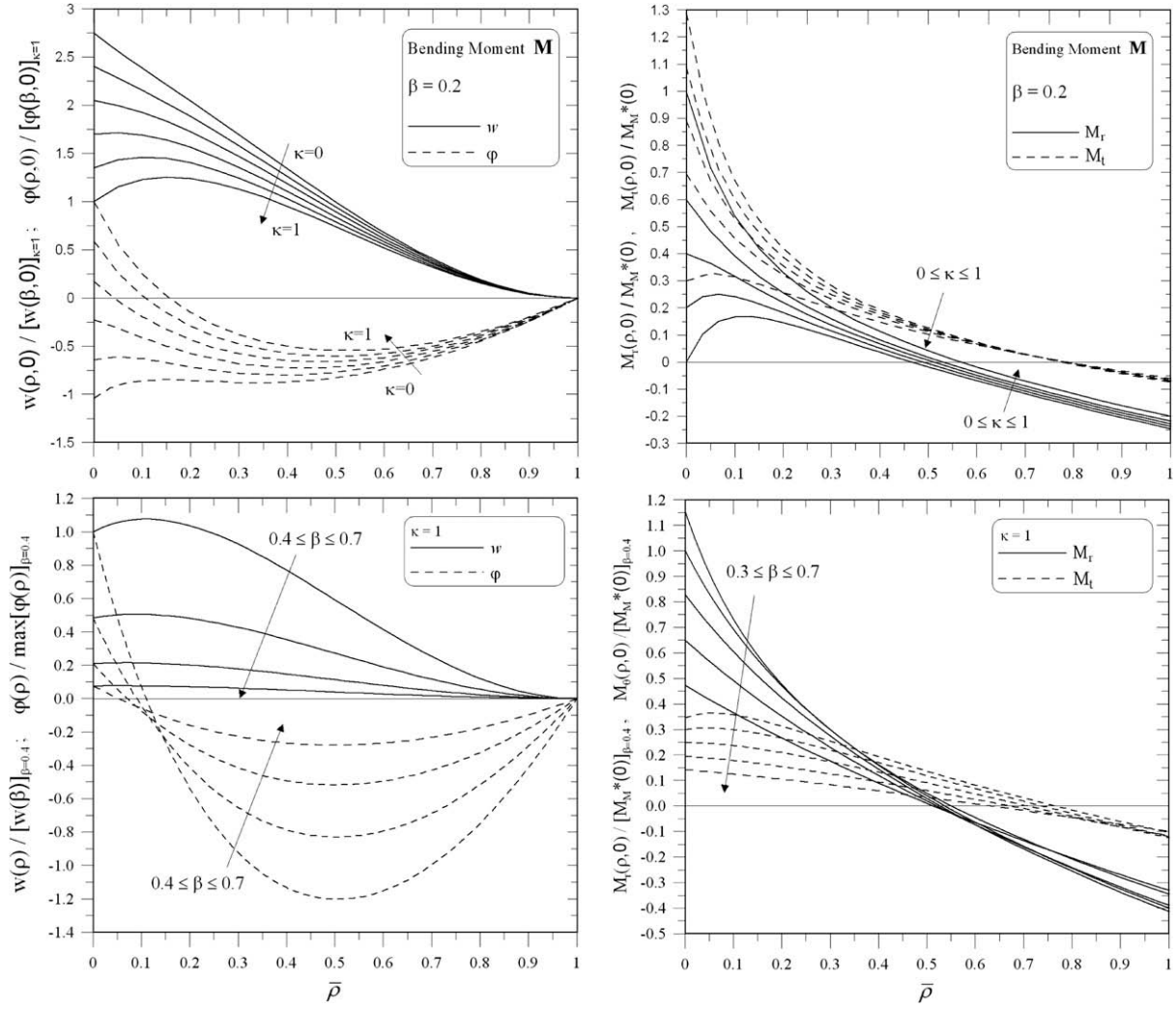

Fig. 4. Theoretical results of bending moment load case ($\theta = 0$).

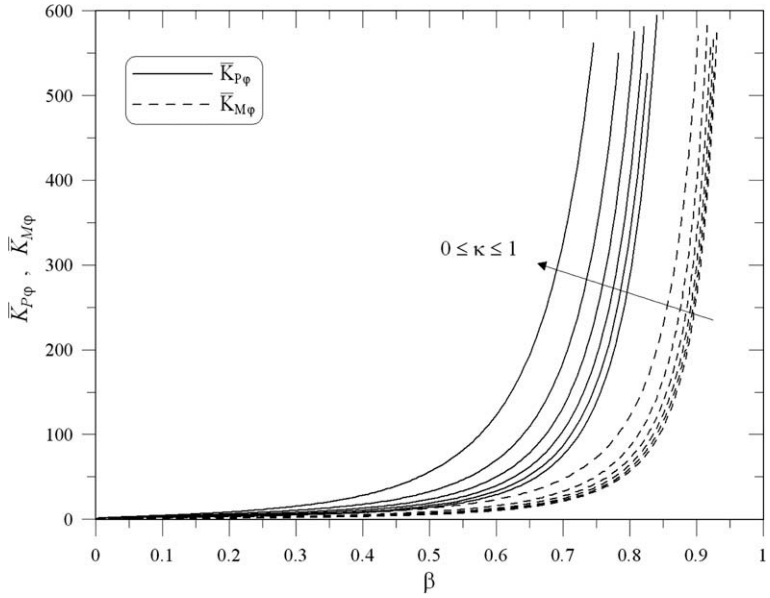

Fig. 5. Curves of $\overline{K}_{P\varphi}$ and $\overline{K}_{M\varphi}$ as functions of $\beta(\nu = 0.3)$.

$$N_{WP} = 2(1+\nu)\beta^2[ln\rho(\rho^2+2ln\beta)+ln\beta(1-\rho^2)] + (3+\nu)\beta^2(1-\rho^2) + 4\beta^2 ln\rho + (1-\nu)[(2ln\rho-1)\rho^2+1]. \quad (15a)$$

$$\varphi(\rho) = \frac{a^2P}{4\pi D}\frac{(\beta^2-1)N_{\varphi P} - 2\kappa\beta^2(\rho^2-1)(\beta^2-1-2ln\ \beta)}{\rho(\beta^2-1)[(1+\nu)\beta^2+1-\nu]};$$

$$N_{\varphi P} = \beta^2(\rho^2-1)[(1+\nu)ln\ \beta+1] - [\beta^2(1+\nu)+(1-\nu)]\rho^2 ln\ \rho. \quad (15b)$$

The moments of this model are given as:

$$M_r(\rho) = \frac{P}{4\pi} \times \frac{[(\nu+1)^2(\ln\beta-\ln\rho)\beta^2-(1-\nu^2)\ln\rho+\nu-1]\rho^2+[(1-\nu^2)\ln\beta+1-\nu]\cdot\beta^2}{\rho^2[\beta^2(1+\nu)+1-\nu]} + \kappa\frac{P}{4\pi}\frac{\beta^2(2\ln\beta-\beta^2+1)[\rho^2(1+\nu)+1-\nu]}{\rho^2(\beta^2-1)[\beta^2(1+\nu)+1-\nu]}. \quad (16a)$$

$$M_t(\rho) = \frac{P}{4\pi}\frac{[(1+\nu)^2(\ln\beta-\ln\rho)\beta^2+(1-\nu^2)\beta^2+(1-\nu^2)\ln\rho+\nu(1-\nu)}{]} \times\rho^2+[(1-\nu^2)\ln\beta+1-\nu]\beta^2\rho^2[\beta^2(1+\nu)+1-\nu] + \kappa\frac{P}{4\pi}\frac{\beta^2(2\ln\beta-\beta^2+1)[\rho^2(1+\nu)-1+\nu]}{\rho^2(\beta^2-1)[\beta^2(1+\nu)+1-\nu]}. \quad (16b)$$

In Fig. 6 the results are shown in the same reference geometry considered in *M*-load case, using dimensionless $\bar{\rho} = (\rho-\beta)/(1-\beta)$ variable. The κ connecting condition constant and β ratio are used, separately, as parameter. By referring to functions in Fig. 6, we have that $M_r(\beta)$ tends to infinity for $\beta \to 0$.

In order to introduce the spot element representing the spot joint and its surrounding region, it is possible to define the stiffness $K^{th}_{Pw}(\kappa)$and $K^{th}_{Mw}(\kappa)$ of Eq. (1) by the ratio of resulting generic force at the peripheral node and the deflection of the nugget:

$$K^{th}_{Pw}(\kappa) = \frac{(\alpha_1+\alpha_2)}{2\pi}\frac{P}{w_1} = \frac{1}{a^2}\frac{8D(\beta^2-1)[\beta^2(1+\nu)+(1-\nu)](\alpha_1+\alpha_2)}{den1};$$

$$den1 = \beta^6(2\kappa\_3-\nu)+\beta^4[-4\kappa(2ln\beta+1)+4(1+\nu)ln\beta(ln\beta+1) + 4(1-\nu)ln\beta+(5+3\nu)]+\beta^2[2\kappa(2ln\beta+1)^2 - 2(1+\nu)ln\beta(2ln\beta+1)-2(3-\nu)ln\beta-(1+3\nu)]-(1-\nu). \quad (17)$$

$$K^{th}_{Mw}(\kappa)] = \frac{M_r(1)}{w_1}a(\alpha_1+\alpha_2) = \frac{8D(\alpha_1+\alpha_2)}{a}\frac{2\kappa\beta^2(1+2ln\beta-\beta^2)+2\beta^2(\beta^2-1)(1+\nu)ln\beta+(1-\nu)[\beta^2(\beta^2-2)+1]}{den2};$$

$$den2 = \beta^6(2\kappa-3-\nu)+\beta^4[-4\kappa(2ln\beta+1)+4(1+\nu)(ln\beta)^2 + 8ln\beta+(5+3\nu)]+\beta^2[2\kappa(2ln\beta+1)^2-4(1+\nu) \times(ln\beta)^2-8ln\beta-(1+3\nu)]-(1-\nu). \quad (18)$$

where $M_r(1)$ is the bending moment at the outer radius; $K^{th}_{Pw}(\kappa)$ is the ratio between the resultant radial shearing force on the outer border of the circular sector having extension $\alpha_1+\alpha_2$ (see Fig. 2) and the deflection at the nugget edge; $K^{th}_{Mw}(\kappa)$ is the ratio between the resultant radial moment on the above-mentioned outer border of the circular sector and the deflection at the nugget edge.

Fig. 7 shows the curves of dimensionless stiffnesses $\overline{K}_{Pw} = K^{th}_{Pw}\cdot a^2/D(\alpha_1+\alpha_2)$ and $\overline{K}_{Mw} = K^{th}_{Mw}\cdot a/D(\alpha_1+\alpha_2)$ as function of β, for various values of κ parameter and $\nu = 0.3$. By referring to functions in Fig. 7, it is confirmed that also $\overline{K}_{Pw}$ and $\overline{K}_{Mw}$ stiffness functions increase with β ratio and tend to infinity when $\beta \to 1$.

3.3. In-plane load T

The external in-plane load *T* is applied (Fig. 1) to the nugget in a direction which lies on the plane containing the sheet. The problem is bi-dimensional, and both equilibrium and compatibility equations are required. In the polar coordinate system (r,θ), the two equilibrium equations and the compatibility equation, in terms of stress, are:

$$\begin{cases}\dfrac{\partial\sigma_r}{\partial r}+\dfrac{1}{r}\dfrac{\partial\tau_{rt}}{\partial\theta}+\dfrac{\sigma_r-\sigma_t}{r}=0\\ \dfrac{1}{r}\dfrac{\partial\sigma_t}{\partial\theta}+\dfrac{\partial\tau_{rt}}{\partial r}+2\dfrac{\tau_{rt}}{r}=0.\end{cases} \quad (19)$$

$$\left(\frac{\partial^2}{\partial r^2}+\frac{1}{r}\frac{\partial}{\partial r}+\frac{1}{r^2}\frac{\partial^2}{\partial\theta^2}\right)(\sigma_r+\sigma_\theta)=0. \quad (20)$$

where σ_r and σ_t are, respectively, the radial and tangential normal stress, and τ_{rt} is the in-plane shear stress. The solution is pursuable introducing the Airy potential function in polar coordinates.

In the polar coordinate system, the radial and tangential normal stresses and shear stress, in terms of *r* and θ, are

$$\sigma_r = \frac{1}{r}\cdot\frac{\partial\phi}{\partial r}+\frac{1}{r^2}\cdot\frac{\partial^2\phi}{\partial\theta^2};\quad \sigma_t = \frac{\partial^2\phi}{\partial r^2};\quad \tau_{rt} = \frac{1}{r^2}\frac{\partial\phi}{\partial\theta}-\frac{1}{r}\cdot\frac{\partial^2\phi}{\partial r\partial\theta}. \quad (21)$$

According to the Airy stress function approach, the governing equation for the circular plate can be written as a bi-harmonic equation of the Airy stress function ϕ . The governing equation in terms of the polar coordinates *r* and θ is

$$\left(\frac{\partial^2}{\partial r^2}+\frac{1}{r}\frac{\partial}{\partial r}+\frac{1}{r^2}\frac{\partial^2}{\partial\theta^2}\right)\left(\frac{\partial^2\phi}{\partial r^2}+\frac{1}{r}\frac{\partial\phi}{\partial r}+\frac{1}{r^2}\frac{\partial^2\phi}{\partial\theta^2}\right)=0. \quad (22)$$

The general solution of the differential Eq. (21) assumes the form:

$$\phi(r,\theta) = f_0(r)+A_0\theta+\left[f_1(r)+\frac{A_1}{2}r\theta\right]\sin\theta+\left[f_1'(r)+\frac{A_1'}{2}r\theta\right]\cos\theta + \sum_{m=2}^{\infty}f_m(r)\sin m\theta+\sum_{m=2}^{\infty}f_m'(r)\cos m\theta. \quad (22)$$

The solution is not influenced here by the elastic radial stiffness in the interface between rigid nugget and inner radius of the plate. Therefore, the solution coincides with the one discussed by Salvini et al. (2000).

Closed form solution of radial displacement $u(\rho,\theta)$ and tangential displacement $v(\rho,\theta)$ are here written:

$$u(\rho,\theta) = u(\rho,0)\cos\theta = \frac{u_1}{2}\frac{[(3-\nu)^2(\beta^2+1)\rho^2ln\rho-(3-\nu)(1+\nu)(\rho^2-1)\beta^2+(1-3\nu)(1+\nu)\rho^4]}{(1+\nu)^2(\beta^2-1)-(3-\nu)^2(\beta^2+1)\ln\beta}\cos\theta \quad (23)$$

$$v(\rho,\theta) = v(\rho,\pi/2)\ \sin\theta == \frac{u_1}{2}\frac{[(3-\nu)^2(\beta^2+1)\rho^2\ln\rho-(3-\nu)(1+\nu)(\rho^2-1)\beta^2+(5+\nu)(1+\nu)\rho^2(1-\rho^2)]}{(1+\nu)^2(\beta^2-1)-(3-\nu)^2(\beta^2+1)\ln\beta}\sin\theta.$$

The stress components $\sigma_r(\rho,\theta)$, $\sigma_t(\rho,\theta)$ and $\tau_{rt}(\rho,\theta)$ are:

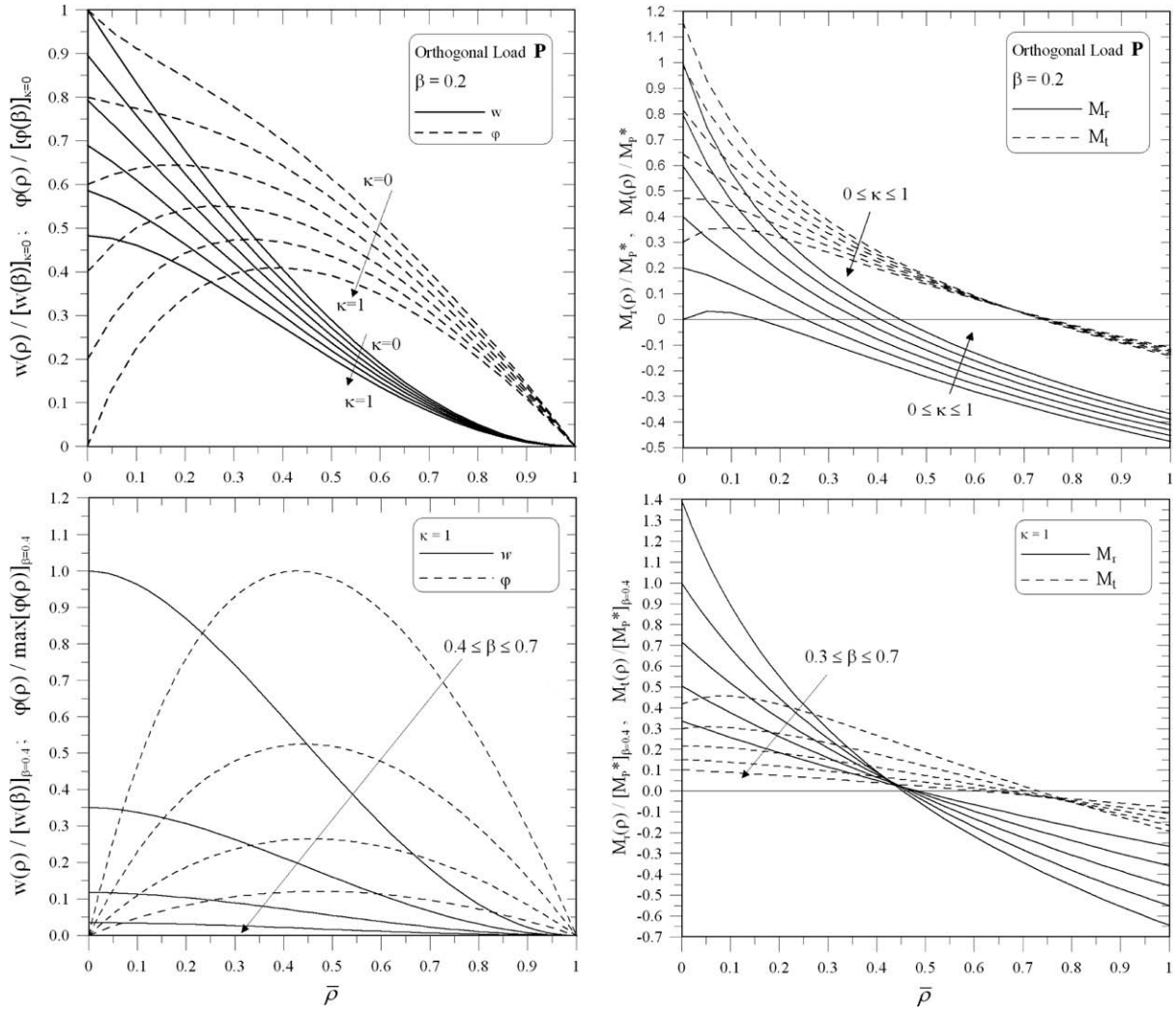

Fig. 6. Theoretical results of orthogonal load case.

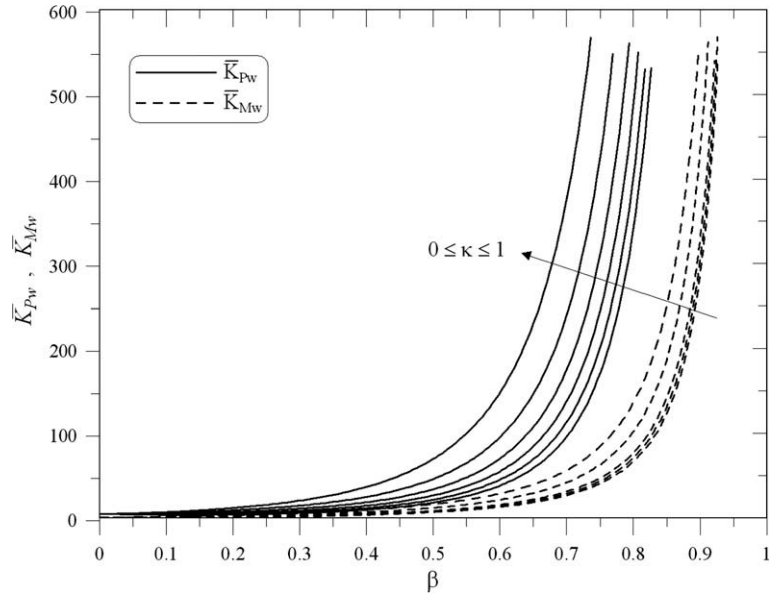

Fig. 7. Curves of $\overline{K}_{Pw}$ and $\overline{K}_{Mw}$ as functions of $\beta(\nu = 0.3)$.

$$\sigma_r(\rho,\theta) = \sigma_r(\rho,0)\cos\theta = \frac{u_1 E[(\nu^2-9)(\beta^2+1)\rho^{-1} - (1+\nu)^2\rho + (3-\nu)(1+\nu)\beta^2\rho^{-3}]}{a(1+\nu)[(1+\nu)^2(\beta^2-1) - (3-\nu)^2(\beta^2+1)\log\beta]} \times \cos\theta; \tag{25a}$$

$$\sigma_t(\rho,\theta) = \sigma_t(\rho,0)\cos\theta = \frac{u_1 E[(3-\nu)(\nu-1)(\beta^2+1)\rho^{-1} - 3(1+\nu)^2\rho + (3-\nu)(1+\nu)\beta^2\rho^{-3}]}{a(1+\nu)[(1+\nu)^2(\beta^2-1) - (3-\nu)^2(\beta^2+1)\log\beta]} \times \cos\theta; \tag{25b}$$

$$\tau_{rt}(\rho,\theta) = \tau_{rt}(\rho,\pi/2)\sin\theta = \frac{u_1 E[(3-\nu)(\nu-1)(\beta^2+1)\rho^{-1}. + (1+\nu)^2\rho - (3-\nu)(1+\nu)\beta^2\rho^{-3}].}{a(1+\nu)[(1+\nu)^2(\beta^2-1) - (3-\nu)^2(\beta^2+1)\log\beta]} \times \sin\theta. \tag{26}$$

In Fig. 8 the results are shown in the same reference geometry considered in *T*-load case, using dimensionless $\bar{\rho} = (\rho-\beta)/(1-\beta)$ variable and β ratio as parameter.

Note that stresses for the spot under a resultant in-plane force acting along *y*-axis can be obtained by substituting $\theta + \pi/2$ for θ in Eqs. (25b) and (26).

In order to introduce the spot element representing the spot joint and its surrounding region, it is possible to define the stiffness $K^{th}_{Fn\,u}(\zeta)$ and $K^{th}_{Ft\,v}(\zeta)$ of Eq. (1) by the ratio of resulting generic force at the peripheral node and the displacement of the rigid nugget. In this function, a new parameter ζ is introduced. ζ parameter $(0 < \zeta \leqslant 1)$ is introduced in order to simulate, as a global effect, the actual local stiffness between the shank of the rivet and the inner radius of the plate. The effect of this parameter is a decrease of in-plane stiffness terms. This term, that in spot weld version is assumed as 1, can be tuned for every rivet typology by means of experimental evidence or results obtained by very accurate FE models.

$$K^{th}_{Fn\,u}(\zeta) = \frac{F_{n2}}{u_1}\zeta = \zeta\frac{t\int_{-\alpha_1}^{\alpha_2}[\tau_{rt}(1,\pi/2)\sin^2\theta - \sigma_r(1,0)\cos^2\theta]ad\theta}{u_1} = \zeta 2tE \times \frac{[(3-\nu)(\beta^2+1)(\alpha_1+\alpha_2) + (1+\nu)(\sin 2\alpha_1 + \sin 2\alpha_2)]}{(1+\nu)[(1+\nu)^2(\beta^2-1) - (3-\nu)^2(\beta^2+1)\ln\beta]} \tag{27}$$

$$K^{th}_{Ft\,v}(\zeta) = \frac{F_{t2}}{v_1}\zeta = \zeta\frac{t\int_{\frac{\pi}{2}-\alpha_1}^{\frac{\pi}{2}+\alpha_2}[\tau_{rt}(1,\pi/2)\sin^2\theta - \sigma_r(1,0)\cos^2\theta]ad\theta}{u_1} = \zeta 2tE \times \frac{[(3-\nu)(\beta^2+1)(\alpha_1+\alpha_2) - (1+\nu)(\sin 2\alpha_1 + \sin 2\alpha_2)]}{(1+\nu)[(1+\nu)^2(\beta^2-1) - (3-\nu)^2(\beta^2+1)\ln\beta]} \tag{28}$$

where $K^{th}_{Fn\,u}(\zeta)$ is the ratio between the resultant radial in-plane loads F_{n2} on the outer border of the circular sector having extension $\alpha_1+\alpha_2$ and centred on $\theta = 0$ – which is the maximum radial nodal loads – and the radial displacement at the nugget edge u_1; $K^{th}_{Ft\,v}(\zeta)$ is the ratio between the resulting tangential in-plane loads F_{t2} on the outer border of the circular sector having extension $\alpha_1+\alpha_2$ and centred on $\theta = \pi/2$ – which is the maximum tangential nodal loads – and the tangential displacement at the rigid nugget edge v_1 for $\theta = \pi/2 (v_1 = u_1)$.

Note that the stiffness functions $K^{th}_{Fn\,u}$ and $K^{th}_{Ft\,v}$ do not depend on θ and they are valid for every direction of application of the resultant in-plane load *T*.

Fig. 9 shows the curves of dimensionless stiffnesses $\overline{K}_{Fn\,u} = K^{th}_{Fn\,u}/tE$ and $\overline{K}_{Ft\,v} = K^{th}_{Ft\,v}/tE$ as function of β, for $\zeta = 1, \nu = 0.3$ and $\alpha_1 = \alpha_2 = \pi/8$. By referring to functions in Fig. 7, it is confirmed that $\overline{K}_{Fn\,u}$ and $\overline{K}_{Ft\,v}$ stiffness functions increase with β ratio and tend to infinity when $\beta \to 1$.

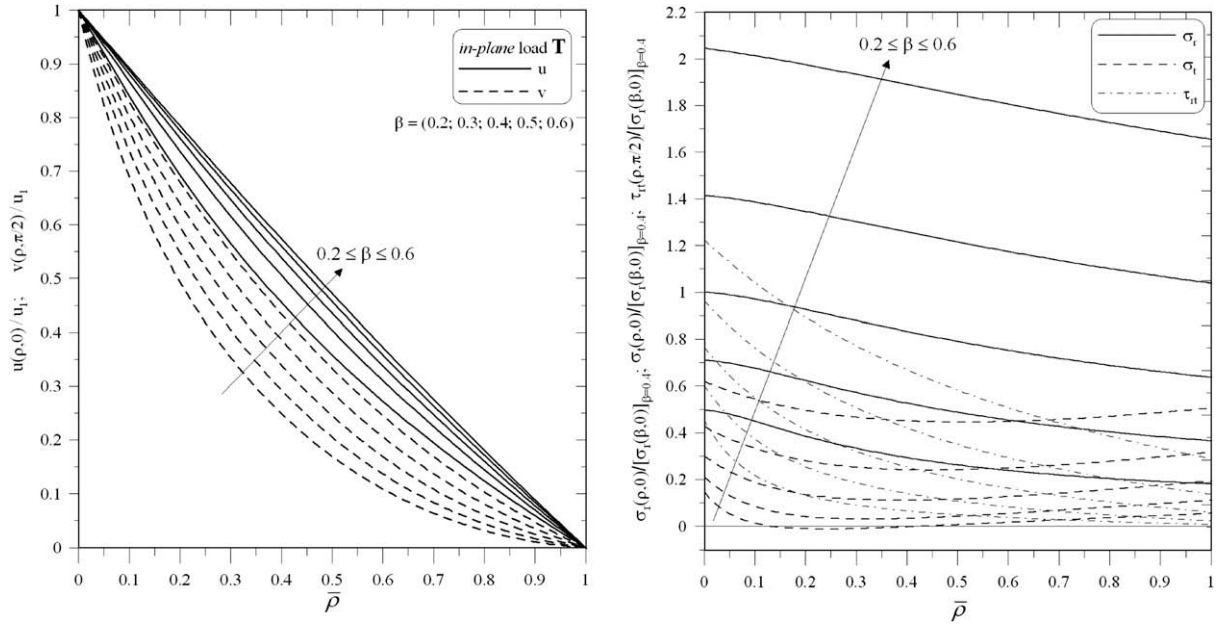

Fig. 8. Theoretical results of in-plane load case.

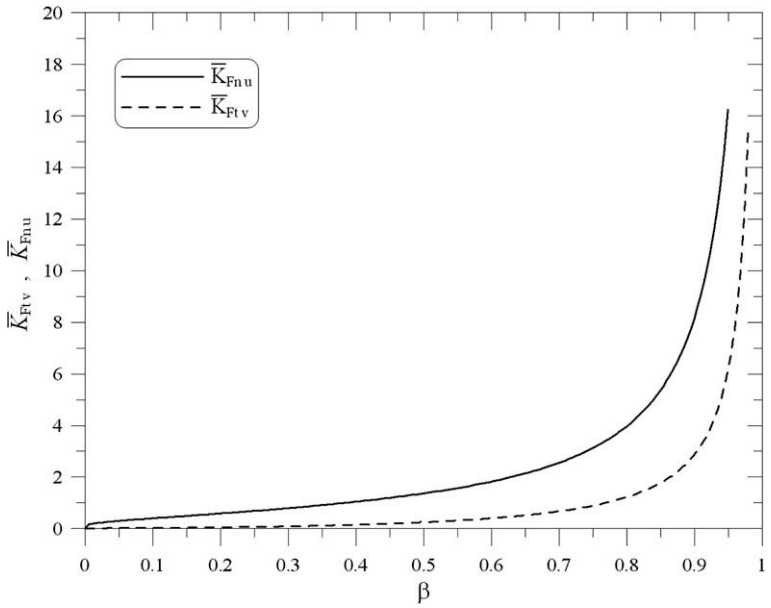

Fig. 9. Curves of $\overline{K}_{Fn\,u}$ and $\overline{K}_{Ft\,v}$ as functions of β $(\nu = 0.3)$.

Finally, with regard to the in-plane stiffness of spot element concerning the torque load condition (a torsion – along z-axis - applied to the nugget), for usual values of $\beta(0.4 < \beta < 0.7)$ and $\alpha_1 + \alpha_2$ (usually between $\pi/20$ and $\pi/4$), it should be pointed out that the torque stiffness of the generic circular sector is quite similar to in-plane stiffness $K^{th}_{Ft\,v}$ of Eq. (28) (for $\beta = 0.7$ and $\alpha_1 + \alpha_2 . = \pi/6$ the difference in stiffness is less than 10%). In the spot element definition only $K^{th}_{Ft\,v}$ is considered within the structural equivalence defined by Eq. (1) with a poor approximation, provided the minor influence of torque loads, especially in a multi-spot structure, with respect to in-plane loads acting on spot joints.

An other facet regards the stiffness of spot element when the self-balanced part of the in-plane loads, i.e. the part of load that does not transit through the spot joint, is applied to the sheet. In this condition, this required stiffness of spot element model is provided by in-plane stiffnesses $K^{th}_{Fn\,u}$ and $K^{th}_{Ft\,v}$, together with stiffness of connected shell elements. Similar considerations are also valid when the self-balanced part of out-of plane loads are applied to the sheet. Nevertheless, in this context, it is important to point out that, in many practical cases, the contribution of the self-balanced part of the loads to the local stresses in spot joints is negligible.

4. First results and discussion: spot weld model

Some results are here discussed, aiming at evaluating the accuracy of results for the spot element in the spot weld version ($\kappa = 1$ and $\zeta = 1$).

Although the spot weld element was validated in other contexts (Salvini et al., 2000; Vivio et al., 2002; Palmonella et al., 2005), further strict analysis is performed here in order to evaluate the correctness of results that can be obtained advantageously using the proposed model and results of the theoretical framework.

A first comparison is performed between closed form solutions of theoretical model and a FE element model whit spot element, varying the mesh refinement and spot element shape. The reference model is an external clamped circular plate having outer diameter d_{plate} and a central rigid nugget having diameter d_{spot}, subjected to P, M and T load cases. A corresponding FE model having shell elements with 6 dofs per node is performed where the central region has been modelled, with the spot element (Fig. 10) in three different shapes and using different mesh size (i.e. a variable number of couple of radial beams N). The spot element has been modelled in circular shape, where the central region has a dimensionless diameter $\beta_{mod} = d_{spot}/d_{mod} = 0.67$, in a rectangular shape (β_{mod} of span sectors varies between 0.47 and 0.67) and in an eccentric shape (β_{mod} of span sectors varies between 0.41 and 0.87), as indicated in Fig. 10. In the three load cases considered here, FE models are subjected, respectively, to the P-load value corresponding to the theoretical maximum deflection $w(\beta)$, to the M-load value corresponding to theoretical maximum slope $\varphi(\beta, 0)$ and to the T-load value theoretical maximum radial displacement $u(\beta, 0)$.

Fig. 11 shows the comparison in term of deflection-distribution curve w and rotation-distribution curve φ as functions of ρ in a steel plate $(\nu = 0.3)$, having ratio $\beta = 0.2$. A very good match between theoretical results and FEA results obtained using the spot weld element $(N = 32)$ is evident.

In Fig. 12a a comparison is reported of results obtained by models having different mesh refinement and spot element shape, in the three load cases considered. Results also confirms the good match with reference theoretical results and a very low influence of model mesh size. Also results obtained using rectangular and eccentric shape of spot element in FE models show a good matching with reference theoretical results. Moreover, in Fig. 12b the map of orthogonal deflection, when a P-load is applied, shows a perfect axisymmetric displacement field, despite of the use of an eccentric or a rectangular spot element.

With the aim of validating the practical use of the spot element, two different simple lap specimens, whose geometry is shown in Fig. 13, have been analysed. The structures are loaded with a tensile load F; the end sections are made rigid. Three different modelling techniques are used (Fig. 14): a refined shell-solid modelling, where the spot region is modelled with 8 node solid elements having 3 dofs per node (model A in Fig. 14) and shell elements are used for metal sheet modelling (the shell-solid assembly has been performed using a suitable set of multipoint constraints, available in the commercial finite element code Ansys®); the well-known modelling which makes use of shells, for the metal sheet, and a simple rigid beam for the spot weld (model B in Fig. 14); the proposed modelling which involves the use of shells, for the metal

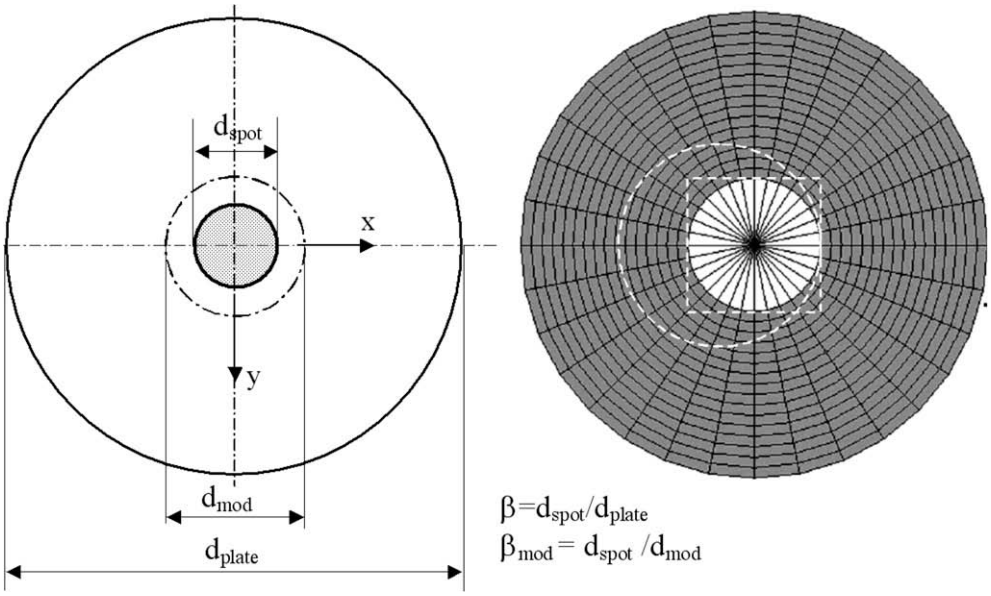

Fig. 10. Reference geometry and its FE model with Spot Element having various shapes.

sheet, and the spot element (model *C* in Fig. 14) with four levels of mesh size. In this latter case the region surrounding the spot was not assumed as circular; the spot model ratio β_{mod} of the span sectors considered varies between 0.44 and 0.63. As previously described, the independent evaluation of the stiffnesses of each sector (Eqs. 9, 10, 17, 18, 27 and 28), which do not depend on θ, allows for managing non-circular spot weld regions; the analytical solution, extended to circumferential portions of the circular

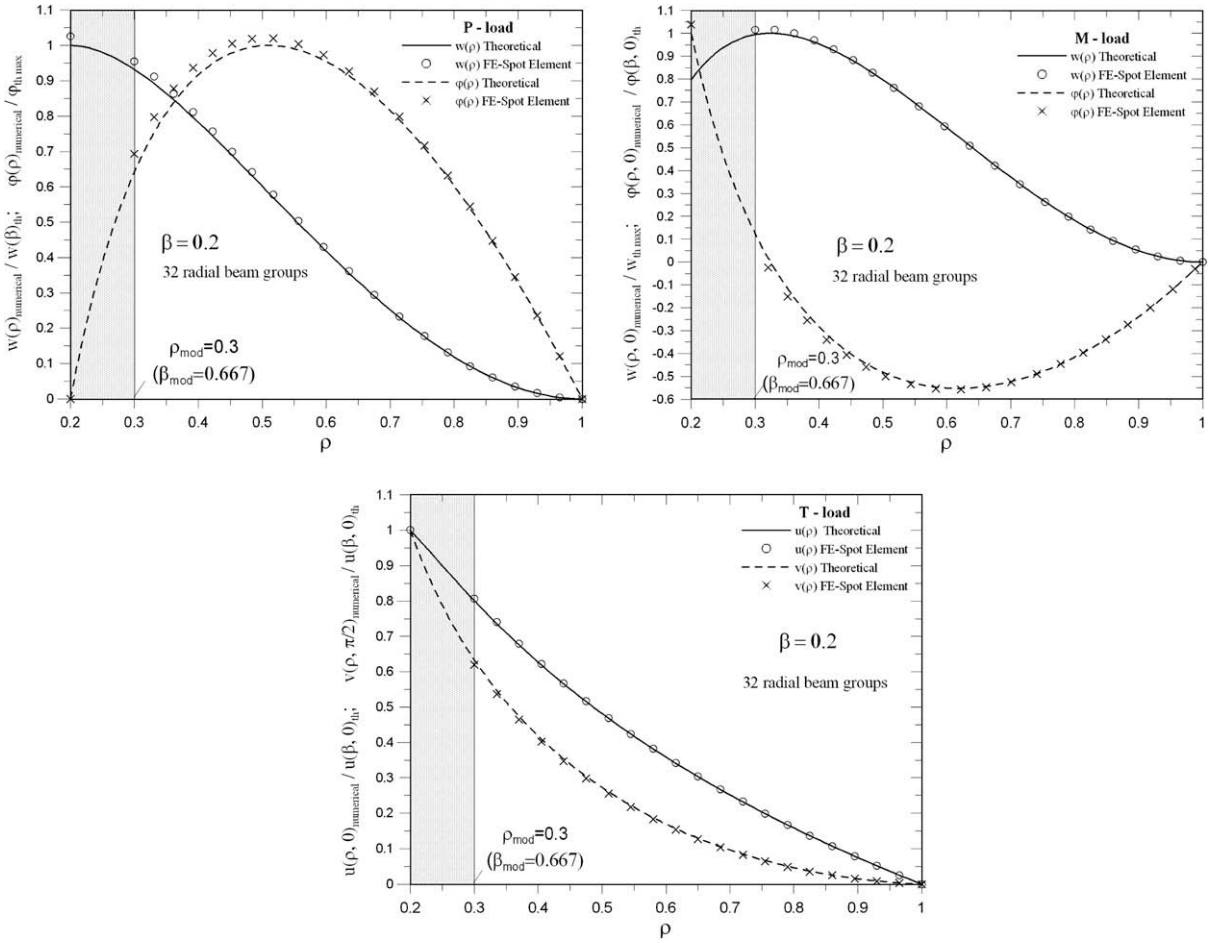

Fig. 11. Deflection-distribution curve and rotation-distribution curve as functions of ρ: comparison between theoretical results and FE results performed using the Spot Element having circular shape.

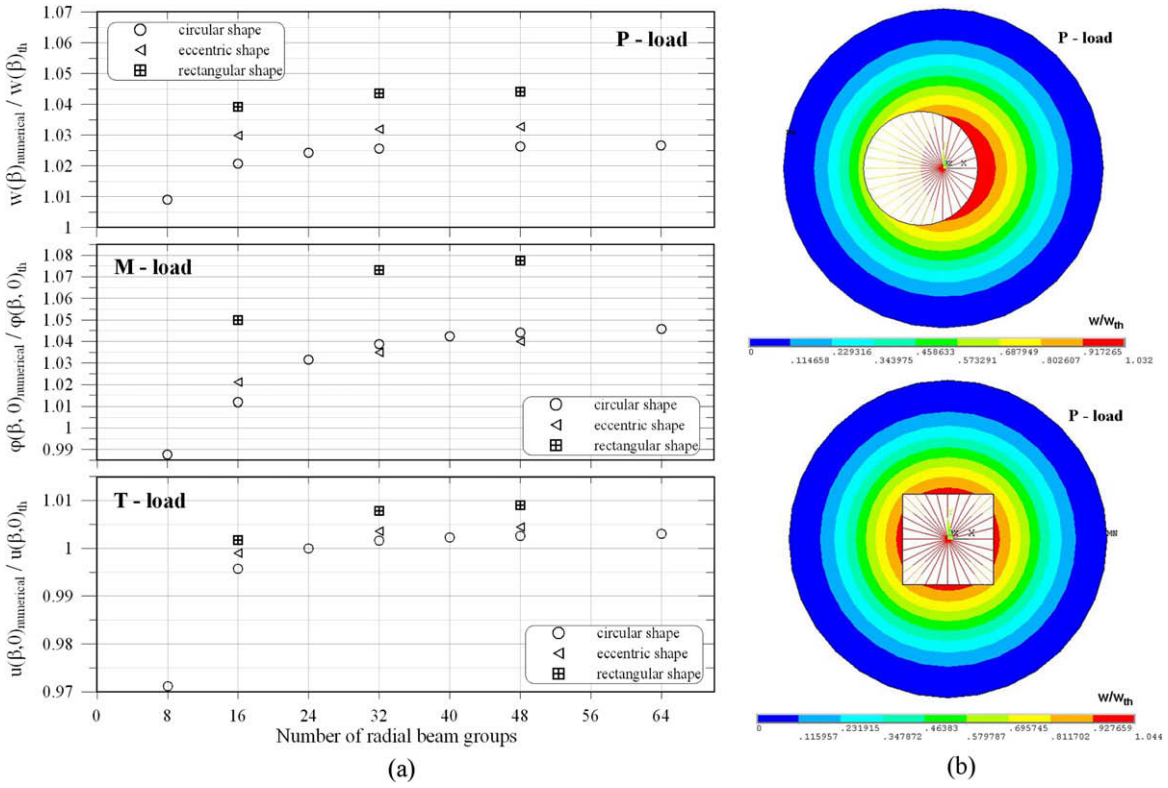

Fig. 12. (a) comparison between theoretical results and FE results performed using the Spot Element having different Spot Element shape and different mesh size. (b) w deflection-distribution map in eccentric and squared Spot Element models (orthogonal P-load).

region surrounding the nuggets and the definition of the corresponding couple of beam T_1 and T_2 (Fig. 2), allows to deal with non-regular-shaped mesh.

The comparison is presented in terms of global stiffness of the specimens, i.e. the ratio between the applied load F and the maximum displacement along the x direction (Fig. 13). Assuming results obtained by model A as reference, Table 1 shows that the error in estimating the global stiffness of the two structure, using the shell-Spot Element model, is very low. It is also confirmed that the influence of the mesh size is very low, and that results obtained with a limited number of nodes in the spot region (i.e. the number of beams used in spot element) remain excellent. Moreover, note that good results of spot element model can be obtained using a high value of spot model ratio β_{mod}, i.e. when the rigid nugget is a great part of the Element. The advantage in local stiffness assessment derives from the intrinsic features of the spot element, which is based on a theoretical framework and allows to overcome the known loss in stiffness simulation of the traditional shell-beam modelling. Nevertheless, it is confirmed that this last traditional modelling (model B) is inadequate to properly simulate both local and global stiffness of the structures, even if it uses a number of degrees of freedom similar or higher than that of spot element model.

With regard to geometry type II of Fig. 13, in Fig. 15 the x -displacement u_x, adimensionalized with the maximum x -displacement picked up by shell-solid model (model A), along x-axis, is reported. The comparison between FE results performed using the different modelling techniques confirms previous considerations.

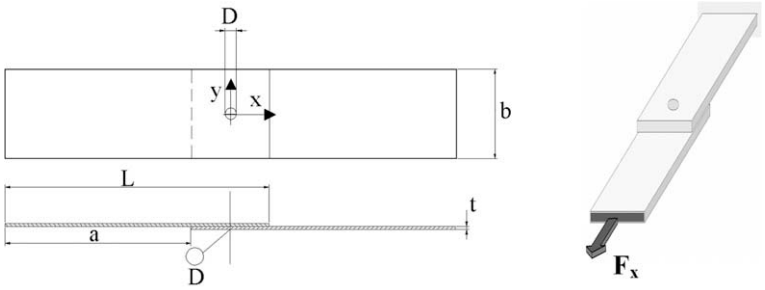

Geometry type	t [mm]	d_{spot} [mm]	a [mm]	b [mm]	L [mm]
I	1.5	6	62.5	48	77.5
II	2	7	50	30	80

Fig. 13. Characteristics of spot welded simple lap specimens (E = 193 GPa, $\nu = 0.3$).

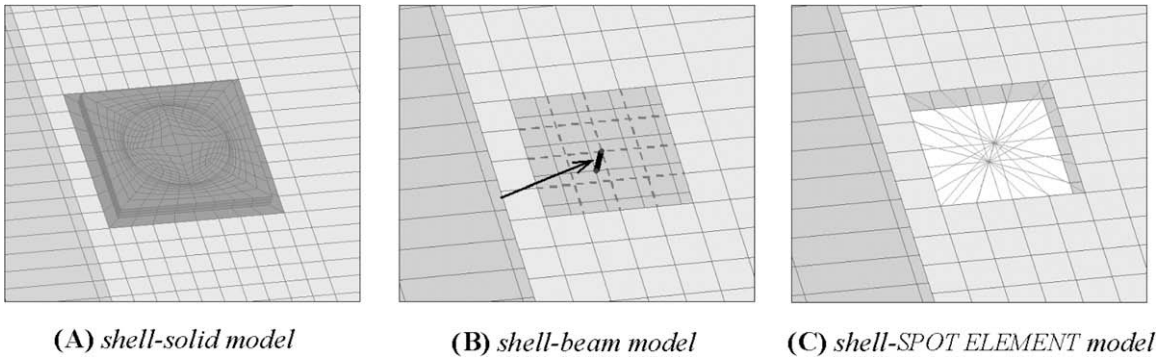

Fig. 14. Different modelling techniques of spot welded simple lap specimen.

Table 1
Comparison among results concerning different model typologies, in terms of global stiffness $K_x^{structure}$ of two different spot welded lap shear specimens. Results of model C regarding four levels of mesh refinement.

Geometry type	Model typology	No. of nodes in spot region	$K_x^{structure}$ [N/mm]	% Error
I	*A*	7265	42264	–
	B	98	30207	−28.5
	C_1	34	41563	−1.7
	C_2	52	41867	−0.9
	C_3	72	42033	−0.5
	C_4	84	42190	−0.2
II	*A*	7265	47595	–
	B	98	33744	−29.1
	C_1	34	46322	−2.7
	C_2	52	47267	−0.7
	C_3	72	47497	−0.2
	C_4	84	47509	−0.2

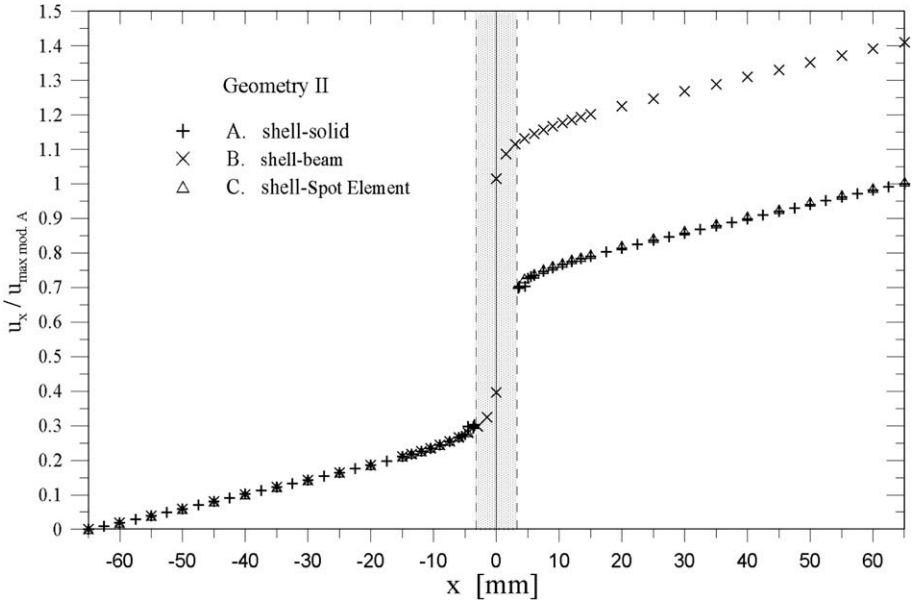

Fig. 15. Dimensionless u_x displacement distribution curve as functions of x: comparison between FE results performed using the different modelling techniques (Geometry type II of simple lap specimens in Fig. 13).

With the aim to validate the actual use of the spot element and corresponding results in FE analyses, a multi-spot T-specimen, whose geometry is shown in Fig. 16, has been analysed. In this case it is important to remark that in a FE model of a multi-spot structure, as the T-specimen or more complex structures, the definition of spot element can be easily performed by creating a macro that can be used as an add-on in any commercial finite element code.

The structure is loaded with two forces respectively acting along x-axis and y-axis, as shown in Fig. 16; the three end sections has been made rigid (as the experimental conditions). In this case the analyses have been performed using only two modelling criteria: each spot weld region has been modelled through the spot element (model *C*) or using a single rigid beam connecting the two sheets (shell-beam model *B*); the corresponding FE models are

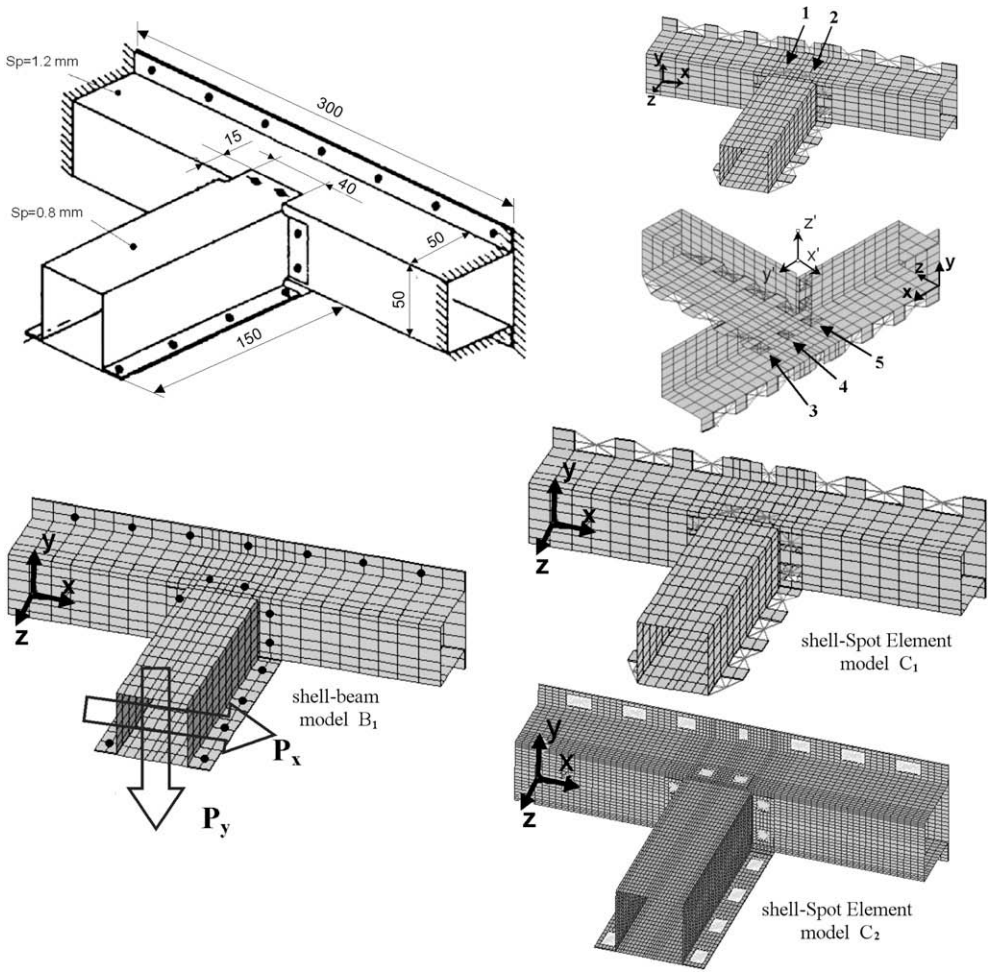

Fig. 16. Characteristics of spot welded T-specimen ($E = 193$ GPa, $\nu = 0.3$) and corresponding FE model typologies.

shown in Fig. 16. In previous example the technique that makes use of spot element has already been compared with the very refined models A, which make use of brick elements.

The comparison has been performed in term of the global stiffness of the joint in two directions, evaluating the ratio between the applied load and the displacement along the corresponding force direction. The stiffness has also been accounted experimentally in the two x and y directions shown in Fig. 16. Results in Table 2 (the values of the last row are the maximum and minimum values accounted in experimental tests), confirm the good results achieved by spot element use. Note that spot element model has a minor influence on mesh size and results obtained by the coarse model C_2 remain good.

A more selective test has been performed in this case, with reference to spot loads. In Table 3 the loads acting on the most stressed spot welds are shown, when a load along y-axis $P_y = 1000$ N has been applied to the T-specimen. It is still possible to point out the relevant difference between results obtained by shell-Spot Element model and shell-beam model; note that the estimate of the torque moment values, in local z-direction, evaluated using model B, are null.

5. First results and discussion: rivet model

Some other results are discussed here, aiming at evaluating the reliability and potential use of the spot element in the simulation of riveted joints. As an example, a cross specimen (Fig. 17) has been firstly modelled by FE, with spot element in rivet version ($\kappa \neq 1$ and $\zeta \neq 1$). A comparison of the proposed procedure (use of spot element) with a very accurate 3D model of rivet has been performed. The 3D FE model, here named *full FEM*, presents a central nugget modelled by means of 8 node solid elements, having 3 dofs per node. The typology of rivet here considered is typical of aeronautic joint, i.e. the blind rivet. A Cherrymax® rivet (as scheme in Fig. 18a) having an aluminium sleeve (QQ-A-430) with a steel stem (AMS 6322) has been considered; the rivet diameter is 5.1 mm. The head and the shop head of the rivet have been simplified in the 3D FE model as two cylinders (Fig. 18b) and their diameters have been considered in the mounted blind rivet: their values are 9.5 mm and 6 mm respectively. These simplifications have a very low influence on joint stiffness behaviour. The diameter of the mounted rivet has been considered as equal to the specimen's hole ($d_{rivet} = d_{hole} = 5.1$ mm).

Contact elements are used in order to account for the connection between the two metal sheet and the heads of rivet, between the hole and the rivet and between the inner part of the two linked plates (Fig. 18c). A classical Coulomb-friction model, with an assumed friction coefficient ($f = 0.1$) was used in all the contact pairs in the model (surface to surface model). A pre-tension of 50 MPa has been imposed to the rivets in the first step of the analysis. The pre-tension value has a low influence on global stiffness of the joint, as confirmed by preliminary FE analysis. Suitable constraints allow for a proper junction between translational dofs of solid elements and rotational dofs of shell elements. During rivet assembly, the rivet undergoes a local deformation and the little

Table 2
Comparison with experimental data of results concerning two different model typologies and two level of mesh refinement, in terms of global stiffness $K_x^{structure}$ of the T-specimen.

Model typology	Model nodes	$K_x^{structure}$ [N/mm]	Error $K_x^{structure}$ [%]	$K_y^{structure}$ [N/mm]	Error $K_y^{structure}$ [%]
B_1	1481	1974	−10.0 ÷ −24.2	1010	−9.0 ÷ −10.1
B_2	12085	1705	−22.2 ÷ −34.5	931	−16.2 ÷ −17.1
C_1	1477	2272	+3.6 ÷ −12.7	1067	−3.9 ÷ −5.0
C_2	11597	2421	+10.4 ÷ −7.0	1105	−0.5 ÷ −1.6
Experimental data		2193 ÷ 2604	–	1111 ÷ 1123	–

Table 3
Comparison among results concerning two different model typologies and experimental data, in terms of loads acting on the most loaded spot welds (upper sheet and lower sheet) of the T-specimen (Fig. 16); $P_y = 1000$ N. Spot local coordinate system $Ox'y'z'$ in Fig. 16.

Model typology	Spot no.		F_X [N]	F_Y [N]	F_Z [N]	M_X [N · mm]	M_Y [N · mm]	M_Z [N · mm]
C_1	1–2	Up.	−2177.0	−460.9	5.4	113.4	8.9	488.9
		Lo.	2177.0	460.9	−5.4	2063.6	−469.8	−488.9
B_1		Up.	−2192.5	−304.5	11.0	217.0	−0.1	0.0
		Lo.	2192.5	304.5	−11.0	1975.6	−304.4	0.0
C_1	3–5	Up.	−1652.2	653.4	4.8	1656.4	592.8	−866.8
		Lo.	1652.2	−653.4	−4.8	−4.2	60.6	866.8
B_1		Up.	−1689.4	500.9	−2.3	1574.8	432.4	0.0
		Lo.	1689.4	−500.9	2.3	114.5	68.6	0.0
C_1	4	Up.	−1107.9	0.0	0.9	16.7	0.0	0.0
		Lo.	1107.9	0.0	−0.9	1091.2	0.0	0.0
B_1		Up.	−1034.3	0.0	−0.2	83.0	0.0	0.0
		Lo.	1034.3	0.0	0.2	951.3	0.0	0.0

gap is made void. Also, this aspect is not taken into account given its low influence in joint stiffness behaviour, still as verified in preliminary FE analysis. In the *full FEM* large displacement hypothesis is considered.

The comparison is presented in terms of global stiffness of the riveted cross specimens $K_z^{structure}$ when a z-load $F_z = 100$N is applied to the specimen. Assuming results obtained by *full FEM* as reference, Table 4 shows results in terms of stiffness error for various values of κ set in spot element definition and different mesh refinement. The central region, modelled with the spot element, has a dimensionless radius $\beta_{mod} = 0.64$.

The comparison points out that a very good definition of the spot element behaviour occurs when κ assumes values between 0.4 and 0.6; according to the specimen's geometry, the ζ parameter, which has a remarkable weight only in the in -plane stiffness of the joint, has very limited impact in terms of local stiffness of the joint, and its variation is not considered here.

Moreover, by observing results on Table 4, the low influence of model mesh size on results is confirmed, also in this case of spot element in rivet version.

In Fig. 19, the dimensionless u_z displacement on cross model (u_z is adimensionalized with respect to the maximum z -displacement picked up by *full FEM*) is reported along x -axis (see coordinate system in Fig. 17). The comparison between FE results performed using the different κ values confirms the good definition of spot element when κ assumes the values before remarked.

With the purpose of evaluating the reliability of results obtained using the spot element, one more example is introduced. A simple riveted lap shear specimen (Fig. 20), very similar to the one described above and here used for experimental investigation, has been modelled by FE with spot element in rivet version (Cherrymax® rivet before described has been used). A comparison with a lap shear FE model having a *full FE* model of rivet, equal to the one before described in cross joint modelling, has been conducted. The free length shown in Fig. 20 is the actual distance between the clamps of the testing machine; in the specimen FE model this distance is considered as the total length, where constraints are applied (here only x translational dofs are free, in the nodes where the load is applied).

The comparison is at first presented in terms of global stiffness of the specimen $K_x^{structure}$, assuming results obtained by *full FEM* as reference. Table 5 shows results in terms of stiffness error for various values of κ and ζ set in spot element definition, for $F_x = 500$ N and $F_x = 1000$ N. The comparison shows that a very good definition of the spot element behaviour occurs when κ assumes values between 0.4 and 0.8 and ζ assumes values between 0.25 and 0.3.

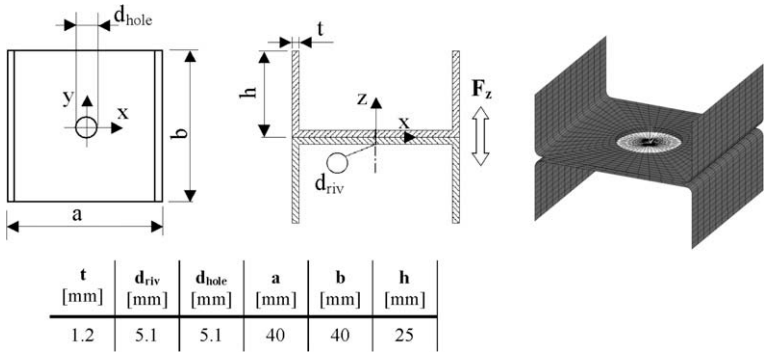

t [mm]	d_{riv} [mm]	d_{hole} [mm]	a [mm]	b [mm]	h [mm]
1.2	5.1	5.1	40	40	25

Fig. 17. Characteristics of riveted cross specimen ($E = 72.8$ GPa, $\nu = 0.27$) and shell-Spot Element model in rivet version ($\beta_{mod} = 0.68$).

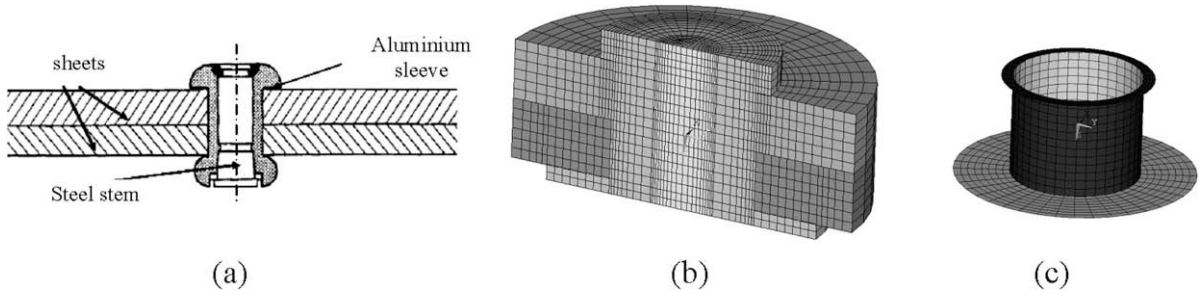

Fig. 18. Cherrymax® rivet joining two sheets (a); detail of *full FE* model (b); contact elements (c) (Rivet radius $b = d_{riv}/2 = 2.6$ mm, sheet thickness $t = 2$ mm, Steel stem diameter 2.2 mm).

Table 4
Percentage error of *z*-axis global stiffness of specimen $K_z^{structure}$ between Spot Element model results and *full FEM* results, for various values of κ and different mesh refinement in Spot Element model.

$N = 48$	κ						
	0	0.2	0.4	0.5	0.6	0.8	1
Error $K_z^{structure}$ [%]	−16.29	−10.24	−3.71	−0.16	3.30	10.68	16.94
$\kappa = 0.5$	*Number of radial beam groups N*						
	96	64	48	32	24	16	
Error $K_z^{structure}$ [%]	−0.07	−0.11	−0.16	−0.50	−0.29	−1.16	

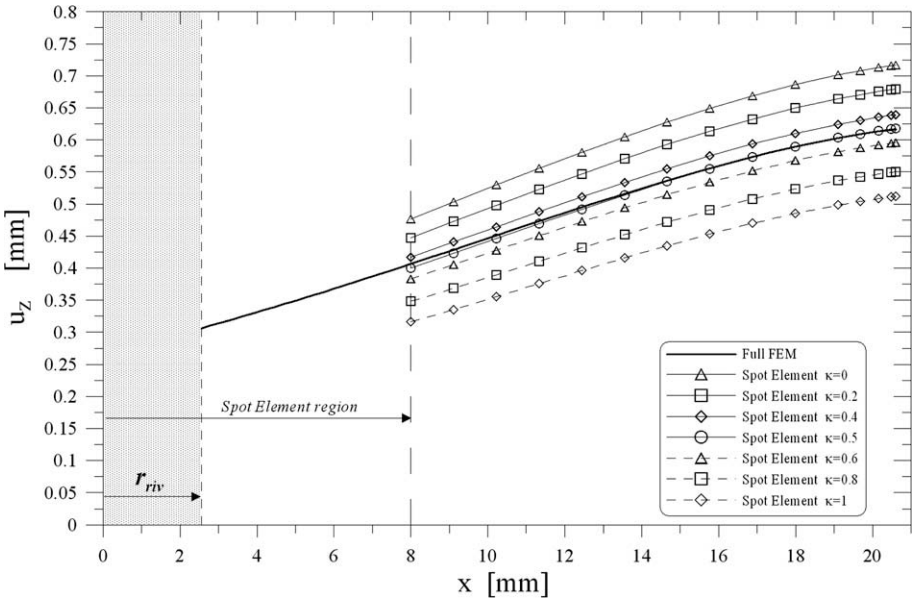

Fig. 19. Dimensionless u_z displacement distribution curve as functions of *x* concerning cross specimen of Fig. 17 ($F_z = 100$ N): comparison between results obtained by *full FEM* and shell-Spot Element model with various values of κ.

Results on Table 6, in terms of percentage error of rivet rotation along *y*-axis φ_{yriv} , indicates that the values of κ 0.4 and 0.6 are the best values. As expected, there are no influence of ζ on rivet rotation.

The results obtained by previous numerical comparisons are also compared with experimental results. The experimental investigation has been performed by testing aluminium tensile -shear specimens before described (Fig. 20).

In order to evaluate the stiffness behaviour of the riveted joint, the test has been performed applying an *x*-force $F_x = 1000$ N. The stiffness of the joint was evaluated using an axial extensometer, with a base distance of 30 mm, which allows to measure the relative *x*-displacement of two points located on the two sheets (as shown in Fig. 20).

In Fig. 21, the u_x displacements distribution curve as a function of *x* is shown; here the comparison is made between results obtained by *full FEM* and shell-Spot Element with various settings of κ and for $\zeta = 0.3$. The experimental data are shown in terms of relative u_x displacement between the two definite points of the extensometer.

The influence on specimen stiffness of κ parameter on displacement is appreciable for positive x values; this is due to the constraint conditions of the model (a full clamping is present for $x = -65$ mm) and to the known low value of the actual stiffness

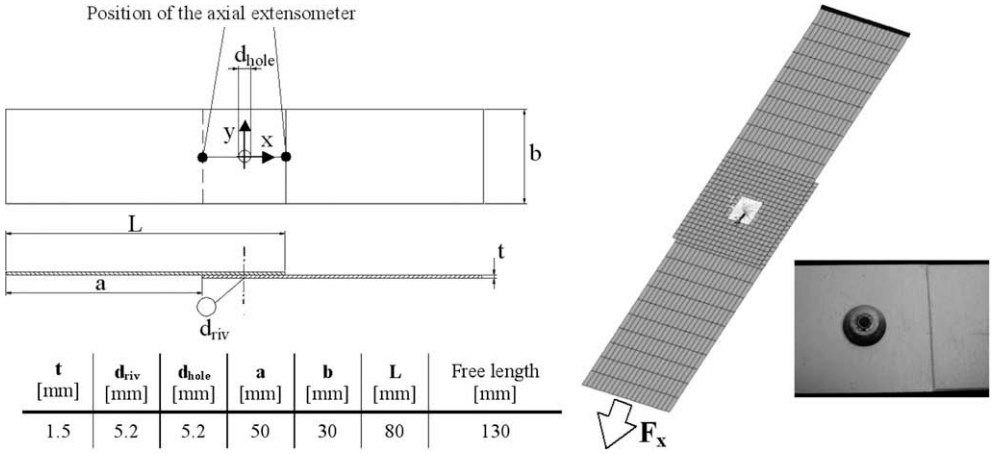

t [mm]	d_{riv} [mm]	d_{hole} [mm]	a [mm]	b [mm]	L [mm]	Free length [mm]
1.5	5.2	5.2	50	30	80	130

Fig. 20. Characteristics of simple lap specimens ($E = 72.8$ GPa, $\nu = 0.27$) riveted with Cherrymax® rivet described above and shell-Spot Element model in rivet version.

Table 5
Percentage error of x-axis global stiffness of specimen $K_x^{structure}$ between Spot Element model results and *full FEM* results.

		κ						
		0	0.2	0.4	0.6	0.8	1	
Error $K_x^{structure}$ [%]								
ζ	0.2	−12.77	−10.85	−8.60	−6.45	−4.55	−3.22	$F_x = 500$ N
	0.25	−5.26	−3.34	−1.09	1.06	2.96	4.30	
	0.3	−0.11	1.82	4.07	6.21	8.11	9.45	
Error $K_x^{structure}$ [%]								
ζ	0.2	−16.32	−14.34	−12.02	−9.80	−7.84	−6.46	$F_x = 1000$ N
	0.25	−8.58	−6.59	−4.27	−2.06	−0.10	1.29	
	0.3	−3.26	−1.27	1.05	3.26	5.22	6.60	

Table 6
Percentage error of rivet rotation along y-axis φ_{yriv} between Spot Element model results and *full FEM* results.

	κ						
	0	0.2	0.4	0.6	0.8	1	
Error φ_{yriv} [%]	−9.80	−4.01	2.73	9.17	14.87	18.89	$F_x = 500$ N
Error φ_{yriv} [%]	−16.47	−10.34	−3.18	3.64	9.69	13.96	$F_x = 1000$ N

of the rivet region if compared to the stiffness of the rest of the structure.

A very good match between the experimental and numerical data is evident. Results obtained using spot element having $\zeta = 0.3$ and $\kappa = 0.4$ show an excellent match with experimental data and *full FEM* results. Note that the best value of κ here found for lap shear specimen is the same of the best value obtained from the analyses conducted on the cross specimen. This confirm the validity of the reference theoretical model here introduced.

6. Conclusions

A new theoretical approach, based on theory of elasticity, and new closed form solutions are presented in order to define the structural behaviour of riveted and spot welded joints. The closed-form solutions lead to the definition of a joint element, useful to FE models of multi-joints structures. The objective is an accurate evaluation of the local stiffness of spot joints in FE analysis, which is fundamental to perform a reliable simulation of multi-joints structures and, consequently, a good estimate of loads acting on spots. On the other hand, a low entry of degrees of freedom is needed when several spot joints are present in a complex structure.

In the paper a new spot element is introduced, based on a new theoretical framework and allowing to precisely evaluate both local and overall stiffness of riveted or spot welded joints. The theoretical model is a circular plate with a central rigid nugget, flexibly connected with the inner radius of the plate, subjected to out-of-plane loads and in-plane loads.

The spot element combines the precision in the simulation with a very limited number degrees of freedom rivet in the overall finite element model of structure. The great advantage provided by introducing the theoretical model presented here makes it possible to encompass spot weld or several different rivet techniques and manufacturing technologies, through the use of two parameters (κ and ζ). This allows to tune the stiffness modelling with the actual structural behaviour of the rivet technique considered, which furthermore depends on several controlled and non-controlled technological parameters.

The method is also able to follow rather accurately all resultant load acting on the spot and the stress state in the surrounding area of each spot. The correct evaluation of loads allows to evaluate local stress or structural stress around rivets or spot welds, using closed form solutions here presented as well as other solutions available in literature.. Moreover, it is possible to follow and simulate changes in local stiffness of spot welds or rivets during fatigue

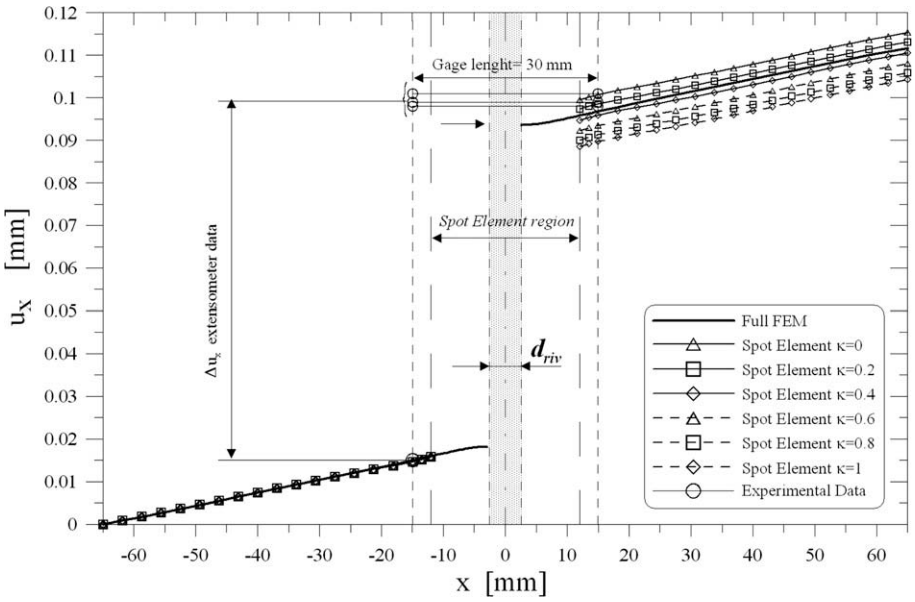

Fig. 21. Displacements u_x distribution curve as functions of x concerning lap shear specimen of Fig. 20 ($F_x = 1000$ N): comparison between results obtained by *full FEM* and shell-Spot Element model with various values of κ and $\zeta = 0.3$.

cycles, managing the mechanical characteristics of the spot element.

In this paper the new spot element has been applied to simulate the structural behaviour of various simple joint geometries and the results have been compared with some experimental data. The comparison clearly show the good accuracy of the results, that can be obtained with a very small number of dofs. The use of a spot element allows to significantly improve the behaviour simulation of spot welded structures and riveted structures, as compared to the widespread use of a simple single-beam element connecting two metal sheets.

References

Al-Emrani, M., Kliger, R., 2003. FE analysis of stringer-to-floor-beam connections in riveted railway bridges. Journal of Constructional Steel Research 59, 803–818.

Deng, X., Chen, W., Shi, G., 2000. Three-dimensional finite element analysis of the mechanical behaviour of spot welds. Finite Elements in Analysis and Design 35, 17–39.

Ho, K.C., Chau, K.Y., 1997. An infinite plane loaded by a rivet of a different material. International Journal of Solids Structures 34 (19), 2477–2496.

Karaoğlu, Ç., Kuralay, N.S., 2002. Stress analysis of a truck chassis with riveted joints. Finite Elements in Analysis and Design 38, 1115–1130.

Langrand, B., Deletombe, E., Markiewicz, E., Drazetic, P., 2001. Riveted joint modelling for numerical analysis of airframe crashworthiness. Finite Element in Analysis and Design 38, 21–44.

Lin, P.C., Wang, D.A., Pan, J., 2007. Mode I stress intensity factor solutions for spot welds in lap-shear specimens. International Journal of Solids and Structures 44, 1013–1037.

Lin, P.C., Pan, J., 2008a. Closed-form structural stress and stress intensity factor solutions for spot welds under various types of loading conditions. International Journal of Solids and Structures 45, 3996–4020.

Lin, P.C., Pan, J., 2008b. Closed-form structural stress and stress intensity factor solutions for spot welds in commonly used specimens. Engineering Fracture Mechanics. doi:10.1016/j.engfracmech.2008.08.005.

Palmonella, M., Friswell, M.I., Mottershead, J.E., Lees, A.W., 2005. Finite element models of spot welds in structural dynamics: review and updating. Computers and Structures 83, 648–661.

Pan, N., Sheppard, S., 2002. Spot welds fatigue life prediction with cyclic strain range. International Journal of Fatigue 24, 519–528.

Radaj, D., 1990. Structural stress, notch stress and stress intensity factor approach for assessment of fatigue strength of spot welded joints. Welding in the World 28 (1/2), 29–39.

Radaj, D., Soegiharto, S., 1990. Structural stress concentration at spot-welded joints: improved model, comparison of results, stress singularity. Welding in the World 28 (9/10), 183–189.

Rupp, A., Grubisic, V., Radaj, D., 1990. Betriebsfestigkeit von Punktschweissverbindunghen. Sonderdruck aus Materialprüfung 32, 1–6.

Rupp, A., Storzel, K., Grubisic, V., 1995. Computer aided dimensioning of spot welded automotive structures. SAE Technical Paper No. 950711, Society of Automotive Engineers, Warrendale, Pa.

Salvini, P., Scardecchia, E., Vivio, F., 1997. Fatigue life prediction on complex spot weld joints. SAE Transaction, Journal of Materials and Manufacturing 106, 967–975.

Salvini, P., Vivio, F., Vullo, V., 2000. A spot weld finite element for structural modeling. International Journal of Fatigue 22, 645–656.

Satoh, T., Abe, H., Nishikawa, K., Morita, M., 1991. On three-dimensional elastic–plastic stress analysis of spot-welded joint under tensile shear load. Transactions of Japanese Welding Society 22, 46–51.

Sheppard, S.D., 1993. Estimation of fatigue propagation life in resistance spot welds. In: Mitchell, M.R., Landgraf, R.W. (Eds.), Advances in Fatigue Lifetime Predictive Techniques, ASTM STP 1211, vol. 2. American Society for Testing and Materials, Philadelphia, pp. 169–185.

Timoshenko, S.P., Woinowsky-Krieger, S., 1959. Theory of plates and shells, 2nd ed. McGraw-Hill, New York.

Urban, M.R., 2003. Analysis of the fatigue life of riveted sheet metal helicopter airframe joints. International Journal of Fatigue 25, 1013–1026.

Vivio, F., Ferrari, G., Salvini, P., Vullo, V., 2002. Enforcing of analytical solution of spot welds into finite element analysis for fatigue-life estimation. International Journal of Computer Applications in Technology 15 (4–5), 218–229.

Vivio, F., Fanelli, P., 2009. A new analytical model for the elastic–plastic behaviour of spot welded joints subjected to orthogonal load. International Journal of Solids and Structures 46 (3–4), 572–586.

Wang, D.A., Lin, S.H., Pan, J., 2005. Stress intensity factors for spot welds and associated kinked cracks in cup specimens. International Journal of Fatigue 27, 581–598.

Xiong, Y., Bedair, O.K., 1999. Analytical and finite element modeling of riveted lap joints in aircraft structure. AIAA Journal 37 (1), 93.

Zhang, S., 1997. Stress intensities at spot welds. International Journal of Fracture 88, 167–185.

Zhang, S., 2001. Fracture mechanics solutions to spot welds. International Journal of Fracture 112, 247–274.